THE UNIVERSITY OF CALGARY

MODELLING OF GAS-SOLID REACTIONS IN POROUS MEDIA

BY

MARLENE KARMANN

A THESIS

SUBMITTED TO THE FACILITY OF GRADUATE STUDIES IN PARTIAL FULFILLMENT OF THE REQUIREMENTS FOR THE DEGREE OF MASTER OF SCIENCE IN ENGINEERING

DEPARTMENT OF CHEMICAL AND PETROLEUM ENGINEERING

CALGARY, ALBERTA, CANADA

APRIL, 1986

ISBN Ø-315-29969-X

THE UNIVERSITY OF CALGARY

FACULTY OF GRADUATE STUDIES

The undersigned certify that they have read, and recommend to the Faculty of Graduate Studies for acceptance, a thesis entitled,

"MODELLING OF GAS-SOLID REACTIONS IN POROUS MEDIA"

submitted by Marlene Karmann in partial fulfillment of the requirements for the degree of Master of Science in Engineering.

M. A. Hastaoglu

Dr. M.A. Hastaoglu, Committee Chairman
Department of Chemical and Petroleum Engineering

Eric L. Tollefson

Dr. E.L. Tollefson
Department of Chemical and Petroleum Engineering

Ayodeji Jeje

Dr. A.A. Jeje
Department of Chemical & Petroleum Engineering

M. Epstein

Dr. M. Epstein
Department of Mechanical Engineering

May 5, 1986

date

ABSTRACT

Mathematical models based on the grain model were written to describe single gas-solid reactions which occur in porous pellets. The models successfully incorporated the effects of external mass transfer, bulk flow, and diffusion through the solid product layer. Structural changes in the pellet (increases or decreases in porosity) due to stoichiometry or density differences between reactant and product solids were also successfully accounted for in the models. The models are capable of describing systems with any type of intrinsic reaction kinetics.

The single-reaction model generated excellent predictions of conversion for non-catalytic and catalytic carbon gasification. An activation energy of 57 kcal/mol was found for non-catalytic carbon gasification. The catalytic effect of nickel on carbon gasification was successfully taken into account by a catalytic rate constant with an activation energy of 50 kcal/mol.

Excellent predictions of conversion for nickel oxide reduction were generated by the model despite severe sintering in the system. The multi-reaction model produced encouraging results for the nickel oxide/carbon/carbon dioxide system.

ACKNOWLEDGEMENTS

I would like to express my gratitude to Dr. M.A. Hastaoglu for his guidance, encouragement, and understanding during the course of this study.

Thanks are also expressed to the Natural Sciences and Engineering Research Council for their financial support.

Finally, I must thank my husband for his unbounded patience and support throughout my graduate studies.

TABLE OF CONTENTS

TABLE OF CONTENTS (Cont'd)

TABLE OF CONTENTS (Cont'd)

LIST OF TABLES

LIST OF TABLES (Cont'd)

LIST OF FIGURES

LIST OF FIGURES (Cont'd)

LIST OF FIGURES (Cont'd)

I INTRODUCTION

Heterogeneous reactions are involved in many industrial processes. Examples of specific applications include coal gasification, extraction of metals from ores, combustion of solid fuels and incineration of solid refuse.

Considerable research effort has been concentrated on the study of gas-solid reactions in the past 40 years. Abundant experimental work has been reported and several models have been proposed, particularly for single-reaction systems. Unfortunately, these models, for the most part, are based on severely restrictive assumptions which hamper their usefulness in describing real situations. In addition, very few results or models have been reported for multi-reaction systems.

Thus, the objectives of this study are as follows:

1) To develop a model which describes a single gas-solid reaction and which is based on few restrictive assumptions.

2) To extend the above model to describe multi-reaction gas-solid systems.

3) To test both models against experimental results for various systems.

The models developed in this study incorporate the structural properties of the reaction system and can be used to find the intrinsic reaction kinetics of the system. Included in the model are the effects of bulk flow, diffusion through the product layer, any type of reaction kinetics, changes in pore structure due to reaction, and external mass transfer resistance.

The single-reaction model describes the general system:

$$A_{(g)} + bB_{(s)} \longrightarrow cC_{(g)} + dD_{(s)}$$

Thus, depending on stoichiometry, the model has the capability of describing gasification reactions (d = 0) or reactions which produce both a gaseous and a solid product.

The multi-reaction model in this study is developed for the following specific reaction system:

$$A_{(g)} + B_{(s)} \longrightarrow 2C_{(g)}$$

$$D_{(s)} + C_{(g)} \longrightarrow E_{(s)} + A_{(g)}$$

With a few modifications, the model could also be used for liquid-solid reactions.

Due to the complexity of the model equations, they are solved numerically. The single-reaction model is tested with noncatalytic and catalytic carbon gasification, as well as with the reaction between nickel oxide and carbon monoxide. The multi-reaction model is tested with the nickel oxide/carbon/carbon dioxide reaction system.

II LITERATURE SURVEY

A. INTRODUCTION

Extensive work has been done over many years in the area of gas-solid reactions. Much of this work has been experimental in nature, examining a wide range of specific reactions. Several models have also been proposed to describe the behaviour of gas-solid reactions. Because of the abundance of literature in this area, this survey will be restricted to only that literature of direct interest to this study. The areas of interest include:

1) Gas-solid reaction models

2) Carbon gasification

3) Nickel oxide reduction

4) Multi-reaction systems.

B. GAS-SOLID REACTION MODELS

For many years, considerable interest has been expressed in the mathematical modelling of gas-solid reactions of the type:

$$A_{(g)} + b\ B_{(s)} \longrightarrow c\ C_{(g)} + d\ D_{(s)}$$

A comprehensive review of the major developments in modelling is given by Ramachandran and Doraiswamy [1].

One of the earliest models to describe gas-solid reactions is the sharp-interface (or shrinking-core) model [2, 3]. This model assumes that the unreacted solid pellet is nonporous and reaction occurs only at a sharp reaction front. This front acts as a boundary, separating the unreacted nonporous core and the porous, completely reacted, product layer. As the reaction proceeds, the unreacted core shrinks.

Numerous improvements to the sharp-interface model have been proposed, including the extension of the model to incorporate any type of reaction kinetics [4, 5]. Rehmat et al [6] have accounted for structural changes in the pellet due to reaction for the non-isothermal case. Recently, Dudukovic [7] examined the case of nonuniform distribution of the solid reactant within the pellet. Park and Levenspiel [8] present a crackling-core model in which the initially nonporous pellet cracks to form a grainy material which, in turn, reacts according to the shrinking-core model. The authors tested the model with the reduction of magnetite with CO.

In another class of models, called the volume reaction models, the pellet is considered to be initially porous. Thus, the reactant gas can diffuse into the pellet and the reaction can take place throughout the whole pellet, rather than at a sharp front. Ramachandran and Dudukovic [9] have discussed the volume reaction model for the case of

non-uniform distribution of the solid reactant. Kimura et al [10] apply the volume reaction model to gas- solid reactions with second-order rate equations.

Ishida and Wen [11] discuss the two-zone model which is a variation of the volume reaction model. In this model, the pellet is porous and reacts as in the volume reaction model. After a period of reaction, the reactant solid at the pellet surface is completely reacted. Thus, a "zone" of completely-reacted product surrounds a "zone" of partially-reacted solid. Ishida and Wen also compared the two-zone model to the shrinking-core model for isothermal and non-isothermal cases [12, 13]. Tone and Wen [14] extended the two-zone model to the case of multiple noncatalytic gas-solid reactions.

Mantri et al [15] and Bowen and Cheng [16] discuss the three-zone model, where the inner zone of the two-zone model is further divided into partially reacted and completely-unreacted zones. Prasannan and Doraiswamy [17] tested the three-zone model with the oxidation of zinc sulfide. Ramachandran and Doraiswamy [18] investigated systems with zero-order dependency on gas and solid and obtain the jumping-zone model. In this model, the reaction zone in the three-zone model remains stationary until the solid in the zone is completely reacted. "The reaction zone then jumps to an adjacent unreacted zone and remains there again till the solid in the new zone is completely exhausted."

Another type of model, called the pore model, was first proposed by Petersen [19]. In his model, Petersen assumed that the porous pellet contains uniformly-sized cylindrical pores which intersect randomly. Several workers since Petersen have studied the uniform-pore model. Ramachandran and Smith [20] tested the model with nickel oxide reduction with carbon monoxide, and with sulfation of calcium carbonate. The effect of bulk flow and reaction reversibility are discussed by Ulrichson and Mahoney [21], who apply the model to chlorination of magnesium oxide.

Pore models for the more realistic case of distributed pore sizes have also been proposed. Hashimoto and Silveston [22] accounted for the pore size distribution with a population balance approach. Gavalas [23] and Bhatia and Perlmutter [24, 25] derived the random pore model in which the reaction surface is assumed to be an overlapping set of cylindrical pores. These pores are characterized by a pore size distribution. Bhatia and Perlmutter applied the random pore model to analyze experimental results of the SO_2 - lime reaction [26] and the CO_2 - lime reaction [27]. Recently, Su and Perlmutter analyzed char oxidation using this model [28].

Su and Perlmutter [29] extended the random pore model to explicitly predict the evolution of the pore size distribution during gasification reactions. Bhatia [30] extended the model to account for distributed pore closure, where small pores are closed first followed by large pores. This accounts for those systems where

conversion is incomplete even where initial porosity would seem to be enough for complete conversion.

Szekely and co-workers [4, 31-36] have proposed the grain model, in which the porous pellet is considered to consist of a closely packed arrangement of nonporous grains. The reactant gas diffuses through the interstices between the grains and reacts with each grain according to the shrinking-core model. The grain model is considered to be realistic in describing physical systems where the solid pellets are agglomerates of grains.

Simplifying assumptions of the original grain model include: restriction of reaction kinetics to first order in gas concentration, constant temperature in the pellet, uniform grain size, pseudo-steady state to describe the concentration of gas A in the pellet, absence of bulk flow, and absence of any variation in the pore structure of the pellet.

Sohn and Szekely [37] demonstrated that reaction rate effects are important and they extended grain model to incorporate Langmuir-Hinshelwood kinetics [38]. Corrections for non-isothermal systems have also been proposed. Ramachandran and Smith [39] considered a temperature gradient in the pellet (the grains are considered small enough to neglect temperature gradients). They proposed the reaction rate constant(s) to be an Arrhenius-type function of temperature. An energy balance on the pellet accounts for non-uniform temperature

distribution. The effect of diffusion through the product layer surrounding the individual grains was studied by Sohn and Szekely [40]. Sampath et al. [41] consider the transient case where pseudosteady state is not valid, which is particularly relevant when a heat balance on the pellet is included in the model.

Nonuniform grain size distribution is studied by Szekely and Propster [42]. They concluded that, although not significant for closely sized grains, size distribution is important in other cases. Sohn and Sohn [43] considered the effect of bulk flow due to volume change on the reaction rate. For initially nonporous pellets, this effect is shown to increase as diffusion becomes rate controlling. Sohn and Bascur [44] extended this to reactions in porous media, for systems where diffusion is in the molecular region, with the same result. Sohn and Braun [45] further extended the idea to internally generated bulk flow due to a separate reaction, applying their results to the gasification of char in an oil shale block [46].

The assumption that has received by far the most attention is that of constant pore structure properties. In many systems, particularly gasification or decomposition, the effect of reaction on the pore structure has been of major interest. Also, sintering can occur at high reaction temperatures in many systems. Early discussions of these topics are given by Calvelo and Cunningham [47], who use the random pore model to determine the diffusivity as a function of porosity. Kim

and Smith [48] studied the effects of reduction and sintering on diffusion in NiO pellets. The sintering effect was considered in terms of removal of pore inter- connections.

Several adaptations to the grain model have been presented to deal with varying structural properties. Similar approaches were presented by Ramachandran and Smith [39], Georgakis et al [49] and Garza-Garza and Dudukovic [50, 51]. The grain radii were considered to be functions of time and position in the pellet and were determined from stoichiometry and density differences between solid reactant and product. Effective diffusivity varies with porosity according to the random pore model. Ramachandran and Smith [39] included the effect of sintering on effective diffusivity. Ranade and Harrison [52] accounted for the effect of both sintering and reaction on structural parameters in terms of relationships for the variation of specific surface area with time. Linder and Simmonson [53] proposed models which accounted for grain size variation and decreasing area available for reaction due to the overlapping of growing product layers.

Recently Sohn and Braun [54, 55] extended the grain model to include multi-reaction systems involving one fluid and two solid reactants or two fluid and one solid reactant. Prasannan et al [56] have incorporated the effect of inert material present in the pellet.

As is evident from the preceding discussion, considerable research effort has been concentrated in improving the grain model. Most

reasearch, however, has been aimed at individual assumptions of the original grain model. Less effort has been concentrated in deriving a version of the grain model which is based on few restrictive assumptions. This is one of the objectives of this study.

In addition, it is evident that most reasearch has been aimed at single-reaction systems. Little has been done to extend the grain model to systems where more than one reaction is occurring. This will be attempted in this study for a specific case involving two consecutive reactions.

C. CARBON GASIFICATION

1) Noncatalytic Carbon Gasification

The general trend in literature has been to describe non-catalytic carbon gasification using a Langmiur-Hinshelwood type of reaction kinetics [57-65]. The overall reaction is described by:

$$C + CO_2 \longrightarrow 2CO$$

If CO_2 and CO are both adsorbed onto the active sites (i.e. C atoms) and the reaction rate is assumed to be proportional to the number of A molecules adsorbed, then the rate is given by [88]:

$$\text{Rate} = k\theta_{CO_2}$$

where θ_{CO_2} is the fraction of sites where CO_2 is absorbed.

The rate of adsorption of CO_2 molecules is proportional to the rate of molecular collision with unoccupied sites:

$$\left.\frac{dn_{CO_2}}{dt}\right|_{ads} = k(1-\Sigma\theta)P_{CO_2}$$

where $\Sigma\theta$ is the total number of occupied sites. The rate of desorption is proportional to the number of CO_2 molecules adsorbed:

$$\left.\frac{dn_{CO_2}}{dt}\right|_{des} = k' \theta_{CO_2}$$

At equilibrium

$$\left.\frac{dn_{CO_2}}{dt}\right|_{ads} = \left.\frac{dn_{CO_2}}{dt}\right|_{des}$$

Thus:

$$\theta_{CO_2} = K_{CO_2} P_{CO_2} (1-\Sigma\theta)$$

In addition, via a similar development

$$\theta_{CO} = K_{CO}P_{CO}(1-\Sigma\theta)$$

Thus:

$$\theta_{CO} + \theta_{CO_2} = \Sigma\theta = (1-\Sigma\theta)\ (K_{CO}P_{CO} + K_{CO_2}P_{CO_2})$$

or:

$$1 - \Sigma\theta = \frac{1}{1+K_{CO}P_{CO}+K_{CO_2}P_{CO_2}}$$

Thus:

$$\text{Rate} = \frac{kK_{CO_2}P_{CO_2}}{1+K_{CO}P_{CO}+K_{CO_2}P_{CO_2}}$$

or:

$$\text{Rate} = \frac{k_1P_{CO_2}}{1 + k_2P_{CO} + k_3P_{CO_2}}$$

where the rate is defined per unit surface area available for reaction.

There is discussion, however, about the mechanism which gives rise to this rate equation. Reif [57] provides a review of some of the more common mechanisms being proposed to describe the overall reaction. Gadsby et al [58] studied the reaction between carbon dioxide and coconut shell charcoal in the temperature range of 700 to 830 °C. They proposed the following sequential set of reactions:

$$CO_{2(g)} \xrightarrow{i_1} (O) + CO_{(g)}$$

$$C + (O) \xrightarrow{j3} CO_{(g)}$$

$$CO_{(g)} \underset{j2}{\overset{i_2}{\rightleftharpoons}} (CO)$$

where $k_1 = i_1$, $k_2 = i_2/j_2$ and $k_3 = i_1/j_3$ are the rate constants in the rate expression.

The most popular mechanism involves two steps:

$$CO_{2(g)} \underset{j_1}{\overset{i_1}{\rightleftharpoons}} (O) + CO$$

$$C + (O) \xrightarrow{j_3} CO_{(g)}$$

In this case, the rate constants are defined as:

$$k_1 = i_1,\ k_2 = j_1/j_3 \text{ and } k_3 = i_1/j_3.$$

This mechanism has been supported by numerous workers [59 - 64].

2) Catalytic Carbon Gasification

Walker et al [66] provide a comprehensive review of the studies investigating catalytic carbon gasification.

One of the earliest mechanisms postulated for catalytic carbon gasification is the oxygen transfer mechanism, described by

$$MeO + CO_2 \longrightarrow MeO.CO_2$$

$$MeO.CO_2 + C \longrightarrow MeO + 2CO$$

where MeO represents the catalyst (which can be metal oxide or metal). In this case, the catalyst is assumed to undergo an oxidation - reduction cycle.

A second mechanism is the electron transfer mechanism. The basis of this mechanism is a transfer of electrons that takes place between the reactant solid and catalyst. This transfer affects the interaction between reactant gas and solid. Long and Sykes [67] discuss this mechanism in detail.

Hastaoglu [65] combined the electron transfer mechanism with the noncatalytic carbon gasification mechanism of Gadsby et al [58]:

$$CO_{2(g)} \xrightarrow{i_1} (O) + CO_{(g)}$$
$$C + (O) \xrightarrow{j_3} CO_{(g)}$$
$$CO_{(g)} \underset{j_2}{\overset{i_2}{\rightleftharpoons}} (CO)$$

Hastaoglu proposed that the catalyst affects the first two steps:

$$CO_{2(g)} + M \underset{j_{3c}}{\overset{i_{1c}}{\longrightarrow}} (O) + CO_{(g)} + M$$

$$C + (O) + M \longrightarrow CO_{(g)} + M$$

where M is the metal concentration and i_{1C} and j_{3C} are catalytic rate constants. If the first catalyzed step is much faster than the second, the rate equation becomes

$$\text{Rate} = \frac{(i_1 + i_{1c}M)\, P_{CO_2}}{1 + i_2/j_2 P_{CO} + i_1/j_3 P_{CO_2}}$$

Another mechanism was proposed by Pettit et al [68] and discussed by Rakszawski et al [69]. In this mechanism, it is postulated that carbon dioxide dissociates over metal catalyst, liberating carbon monoxide and

adsorbing an oxygen atom to the catalyst. The oxygen atom diffuses to a carbon atom and reacts to form the second carbon monoxide molecule.

D. NICKEL OXIDE REDUCTION

It is generally agreed in literature that the form of the reaction rate for nickel oxide reduction is first order with respect to carbon monoxide concentration. Unfortunately, few investigators have studied nickel oxide reduction at temperatures which are of interest to this study (ie above 800°C).

Szekely and Lin [70] investigated the temperature range of 847 to 1099 °C. Their results were interpreted using the grain model in order to deduce the rate constant. The results indicated an activation energy of 4 kcal/mole, but showed considerable scatter.

Krasuk and Smith [71] investigated nickel oxide reduction between 566 and 796 °C. In the temperature range of 566 to 682 °C, an activation energy of 47 kcal/mol was reported. Above 682°C, the rate constant is essentially independent of temperature ($\Delta E = 0$). Krasuk and Smith suggested that the zero activation energy at higher temperatures may be due to the sintering of nickel.

Several other investigations of nickel oxide reduction have been reported: Oates and Todd [72], Bielanski et al [73], Mine et al [74].

However, the temperature ranges of these investigations were far below the range of interest for this study.

E. MULTI-REACTION SYSTEMS

The system of interest in this system is described by the following two equations:

$$C + CO_2 \longrightarrow 2CO$$

$$MeO + CO \longrightarrow Me + CO_2$$

where Me refers to nickel for this study.

There are two schools of thought in the literature about coupled reactions of this type. Some investigators support the theory that the mechanism is described by the two reactions given above. Others believe that, in addition to the above reactions, a solid-solid reaction between the metal oxide and carbon occurs.

Rao [75] provides a good review of both mechanisms. After investigating the reduction of hematite with carbon, Rao supported the gas phase mechanism, claiming that the solid-solid reaction is insignificant to the overall reaction rate. Pavlyuchenko et al [76]

used a tracer method with C^{14} isotope to investigate the diffusion of solids during carbon reduction of nickel and copper oxides. They concluded that the rate of diffusion of the solids is too slow to account for the reaction rate and supported a gas phase mechanism.

El-Guindy and Davenport [77] studied the reduction of ilmenite and graphite. They concluded that up to 1020°C the solid-solid reaction mechanism was important. Above 1020°C, the gas phase mechanism predominated. Yun [78] also supports the solid-solid mechanism and has studied ferric oxide reduction by carbon. He claims that the diffusion of metal ions is the rate -determining process in the reduction reaction. Hastaoglu [65] supported the solid-solid mechanism. He investigates the reaction between nickel oxide and carbon in atmospheres of carbon dioxide, carbon monoxide and nitrogen. He concludes that a very fast initial reduction rate is due to solid-solid reaction at the contact points of the grains.

III MATHEMATICAL FORMULATION OF THE MODELS

A. INTRODUCTION

The model equations derived in this study are based on the grain model of Szekely and co-workers [4, 31-36]. The grain model was chosen in this study as it realistically describes the solid pellets used in the experimental studies (i.e. powders of the solid reactants were pressed to form pellets). In the grain model, a solid porous pellet is considered to consist of a closely-packed arrangement of nonporous spherical grains, as shown in Figure 1. The model equations are written for disc-shaped pellets but could be easily converted for cylindrical or spherical pellets.

The reactant gas passes through the interstices between the grains and reacts with individual grains according to the shrinking core model. At each grain, the reaction begins at the surface. As the reaction progresses, the reaction front moves into the grain, separating the product layer and the unreacted core. The rate of reaction is controlled by several factors [4]:

(1) External mass transfer of the gaseous reactant across the gas film from the bulk gas stream to the pellet surface.

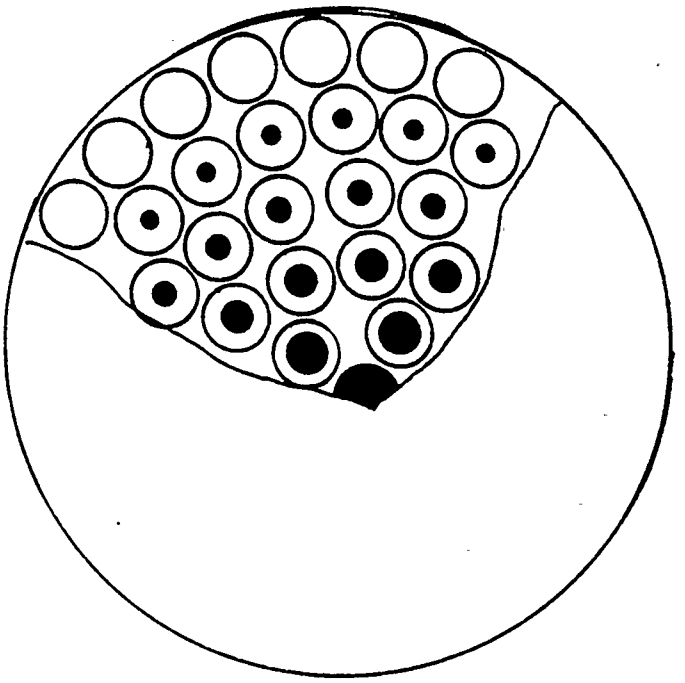

Figure 1 - THE GRAIN MODEL

(2) Diffusion of the gaseous reactant into the pellet through the pores between the grains.

(3) Diffusion of the gaseous reactant through the product layer surounding individual grains.

(4) Reaction of the gaseous and solid reactants, as controlled by the intrinsic reaction kinetics.

(5) Diffusion of the gaseous product through the product layer surrounding individual grains.

(6) Diffusion of the gaseous product out of the pellet through the pores between the grains.

(7) External mass transfer of the gaseous product from the pellet surface to the bulk gas stream.

Simplifying assumptions which are implicit in the models derived in this study include:

(1) The reaction system is isothermal.

(2) Sintering does not occur to any significant degree.

(3) The size of the pellet does not change during the reaction.

(4) The pseudo-steady state assumption is valid in considering the concentrations of A and C in the pellet.

Assumption (1) is considered to be valid in this study since the heats of reaction for the systems under investigation are small [89]. With the proper mathematical formulations, assumptions (1) to (4) could be incorporated into the model.

In the following section, model equations are developed for the single-reaction system described by:

$$A_{(g)} + b\ B_{(s)} \longrightarrow c\ C_{(g)} + d\ D_{(s)}$$

The single-reaction model is then extended to describe the multi-reaction system:

$$A_{(g)} + B_{(s)} \longrightarrow 2\ C_{(g)}$$
$$D_{(s)} + C_{(g)} \longrightarrow E_{(s)} + A_{(g)}$$

Finally, several auxiliary equations for the two models are discussed.

B. SINGLE-REACTION MODEL

In this section, the model which describes a single-reaction system is developed. The system is governed by equation (1):

$$A_{(g)} + b\ B_{(s)} \rightarrow c\ C_{(g)} + d\ D_{(s)} \qquad (1)$$

The main model equations are based on the following laws:

1) Conservation of gaseous reactant A

2) Conservation of solid reactant B

3) Conservation of gaseous product C.

To determine the conservation equation for gaseous reactant A, consider a volume element of thickness ΔR at the position R in the pellet, as in Figure 2. A material balance on reactant A results in:

$$N_A S_E|_{R+\Delta R} - N_A S_E|_R - V_E S_V f(C_{Ai}, C_{Ci}) = 0 \qquad (2)$$

where S_E and V_E are the surface area at the given boundary and the volume of the element respectively.

In equation (2), the first term refers to the amount of A entering the volume element; the second to the amount of A leaving the element. The third term accounts for the consumption of A in the element due to

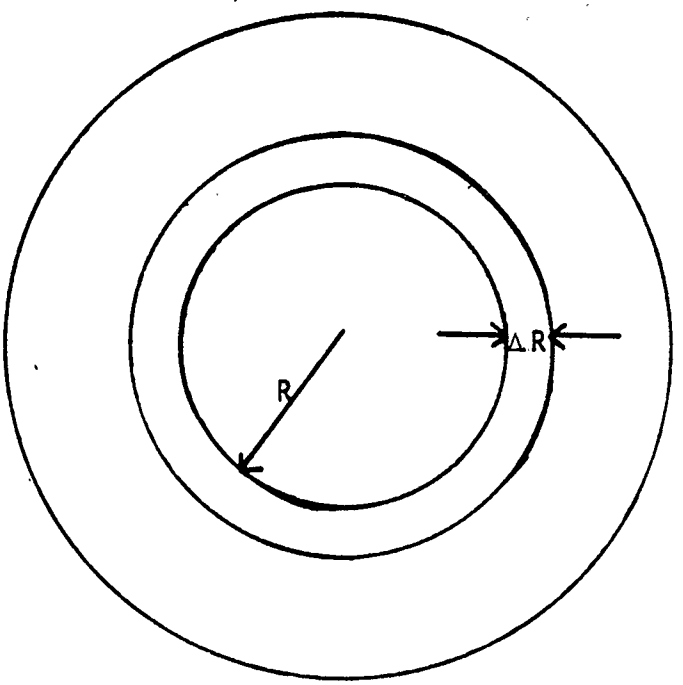

Figure 2 - VOLUME ELEMENT FOR CONSERVATION EQUATIONS

reaction. The absence of an accumulation term is due to the pseudo-steady state assumption, discussed in section A above. In the third term, $f(C_{Ai}, C_{Ci})$ is the intrinsic reaction rate per unit surface area and can describe any type of reaction kinetics (eg. power law, Langmuir-Hinshelwood, etc.).

C_{Ai} and C_{Ci} refer to the concentrations of A and C respectively at the reaction front in the grain where the reaction takes place. The surface area in the pellet available for reaction per unit pellet volume, S_v, is given by:

$$S_v = 3(1-\varepsilon_o)\frac{r_c^2}{r_o^3} \qquad (3)$$

where r_c is the radius of the reaction front in the grain and r_o is the initial grain radius.

Assuming constant total concentration, the molar flux N_A is given by:

$$N_A = x_A(N_A + N_C) - D_{eA}\frac{dC_A}{dR} \qquad (4)$$

where

D_{eA} = the effective diffusivity of A in the pores between the grains

C_A = the concentration of A in the pores between the grains

x_A = the mole fraction of A = $C_A/(C_A + C_C)$

Stoichiometry of the reaction dictates that

$$N_C = -cN_A \tag{5}$$

Thus

$$N_A = -\frac{D_{eA}}{1-(1-c)x_A}\frac{dC_A}{dR} \tag{6}$$

For a disc-shaped pellet (the development is similar for cylindrical and spherical pellets).

$$S_E = \frac{\pi}{4} \text{diap}^2 \tag{7}$$

and

$$V_E = \frac{\pi}{4} \text{diap}^2 \, \Delta R \tag{8}$$

where diap is the pellet diameter.

If equations (6), (7) and (8) are substituted into equation (2), the result is:

$$\left. \frac{D_{eA}}{1-(1-c)x_A} \frac{dC_A}{dR} \right|_{R+\Delta R} - \left. \frac{D_{eA}}{1-(1-c)x_A} \frac{dC_A}{dR} \right|_{R} - \Delta R \, 3(1-\varepsilon_o) \frac{r_c^2}{r_o^3} f(C_{Ai}, C_{Ci}) = 0 \tag{9}$$

If ΔR is allowed to go to zero, equation (2) becomes:

$$\frac{1}{1-(1-c)x_A} \frac{\partial}{\partial R} \left(D_{eA} \frac{\partial C_A}{\partial R} \right) - 3(1-\varepsilon_o) \frac{r_c^2}{r_o^3} f(C_{Ai}, C_{Ci}) = 0 \tag{10}$$

In order to determine the equation for the conservation of C, consider a material balance of product gas C across the same volume element in Figure 2. The conservation of C becomes:

$$N_C S_E\Big|_{R+\Delta R} - N_C S_E\Big|_R + V_E S_V c f(C_{Ai}, C_{Ci}) = 0 \qquad (11)$$

The molar flux N_C is given by (assuming constant total concentration):

$$N_C = x_C(N_A + N_C) - \frac{D_{eC} dC_C}{dR} \qquad (12)$$

with

$$N_A = -1/c\ N_C \qquad (13)$$

Thus

$$N_C = -\frac{D_{eC}}{1-(1-1/c)x_C} \frac{dC_C}{dR} \qquad (14)$$

and equation (11) becomes:

$$-\frac{1}{1-(1-1/c)x_C} \frac{\partial}{\partial R}\left(D_{eC} \frac{\partial C_C}{\partial R}\right) + 3c(1-\varepsilon_o) \frac{r_c^2}{r_o^3} f(C_{Ai}, C_{Ci}) = 0 \qquad (15)$$

The concentrations of A and C at the reaction front (C_{Ai} and C_{Ci}) are found by considering the flux of A and C through the product layer surrounding the individual grains. In this case, for reactant gas A,

$$N_A = - D_{gA} \frac{dC_A}{dr} \tag{16}$$

where D_{gA} is the diffusivity of A in the porous product layer. Approximating the differential by a difference results in

$$N_A = - D_{gA} \frac{C_A - C_{Ai}}{r_g - r_c} \tag{17}$$

or

$$\frac{dn_A}{dt} = -4\pi r_g r_c D_{gA} \frac{C_A - C_{Ai}}{r_g - r_c} \tag{18}$$

where n_A is the number of moles of A.

A similar expression can be developed for the flux of C through the product layer:

$$\frac{dn_C}{dt} = -4\pi r_g r_c D_{gC} \frac{C_C - C_{Ci}}{r_g - r_c} \tag{19}$$

In addition, the reaction kinetics dictates that

$$\frac{dn_A}{dt} = -4\pi r_c^2 \, f(C_{Ai}, C_{Ci}) \tag{20}$$

and

$$\frac{dn_C}{dt} = 4c\pi r_c^2 \, f(C_{Ai}, C_{Ci}) \tag{21}$$

Simultaneous solution of equations (9), (15), (18), (19), (20) and (21) results in quantities for C_A, C_C, C_{Ai}, C_{Ci}, dn_A/dt and dn_C/dt.

The final conservation equation, for the solid reactant B, can be derived from stoichiometry as:

$$\frac{dn_B}{dt} = b \frac{dn_A}{dt} \tag{22}$$

The number of moles of B per grain, n_B, is given by:

$$n_B = 4/3\ \pi \frac{\rho_B}{M_B} r_c^3 \tag{23}$$

where ρ_B and M_B are the true density and the molecular weight of B respectively. Thus

$$\frac{dn_B}{dt} = 4\pi \frac{\rho_B}{M_B} r_c^2 \frac{dr_c}{dt} \tag{24}$$

Substituting equations (20) and (24) into equation (22) results in the conservation equation which governs the movement of the reaction front.

$$\frac{\rho_B}{M_B} \frac{dr_c}{dt} = - bf(C_{Ai}, C_{Ci}) \tag{25}$$

Equation (25) is solved to find the reaction front radius at any time during the reaction.

As the reaction proceeds, the radius of the grain, r_g, will change in general. This is caused by a combination of reaction stoichiometry (i.e., b moles of B react to produce d moles of solid D) and the density differences between solid reactant and product. The change of the grain radius is determined by a material balance on the product layer surrounding the grain. For spherical grains:

$$b\,(r_g^3 - r_c^3)\,\frac{\rho_D}{M_D}\,(1-\varepsilon_D) = d(r_o^3 - r_c^3)\,\frac{\rho_B}{M_B} \qquad (26)$$

where ε_D is the porosity of the product layer. Thus, from equation (19) the grain radius can be determined at any time and position in the pellet once the reaction front radius is known.

The porosity of the pellet necessarily changes as a result of swelling or shrinking of the grains. The volume of the pellet at any time is given by:

$$V_p = n_g\,\frac{4\pi}{3(1-\varepsilon)}\,r_g^3 \qquad (27)$$

The initial pellet volume is:

$$V_{po} = n_{go}\,\frac{4\pi}{3(1-\varepsilon_o)}\,r_o^3 \qquad (28)$$

where n_g and n_{go} are number of grains at any time and initially respectively. Since the pellet volume and the number of grains are assumed to remain constant:

$$\frac{1 - \varepsilon}{1 - \varepsilon_o} = \frac{r_g^3}{r_o^3} \tag{29}$$

The change in porosity will in turn affect the effective diffusivity in the pores. With $\tau = 1/\varepsilon$ the random pore model [79] gives the effective diffusivity as:

$$D_e = D \frac{\varepsilon}{\tau} = D\varepsilon^2 \tag{30}$$

where τ is tortuosity and D is composite diffusivity accounting for Knudsen and bulk molecular diffusivities.

The model formulated above is subject to the following initial and boundary conditions:

1) There is no reaction before time t = 0;

$$r_c = r_o \text{ for all R at } t = 0 \tag{31}$$

2) There is symmetry at the center of the pellet;

$$\frac{\partial C_A}{\partial R} = 0 \quad \text{at } R = 0 \tag{32a}$$

$$\frac{\partial C_C}{\partial R} = 0 \quad \text{at } R = 0 \tag{32b}$$

3) The diffusive flux into the pellet equals the convective flux across the external gas film;

$$\frac{D_{eA}}{1-(1-c)x_A} \frac{\partial C_A}{\partial R} = h(C_{Ab} - C_A) \quad \text{at } R = R_p \tag{33a}$$

$$\frac{D_{eC}}{1-(1-1/c)x_C} \frac{\partial C_C}{\partial R} = h(C_{Cb} - C_C) \quad \text{at } R = R_p \tag{33b}$$

where C_{Ab} and C_{Cb} are the bulk concentrations of A and C respectively.

In general, in order to make the model useful for comparison to experimental results, the overall conversion of the solid reactant (as determined by the weight loss of the pellet) is needed. For isothermal conditons, the local conversion at any point R in the pellet and any time t is given by:

$$x(R,t) = 1 - \frac{r_c(R,t)^3}{r_o^3} \tag{34}$$

Equation (34) compares the amount of solid reactant consumed to the initial amount of solid reactant present initially, on an individual grain basis.

If the number of grains is assumed to remain constant throughout the reaction, the overall conversion of the solid reactant is found by integrating over the total number of grains in the pellet [35]. Thus, the overall conversion is given by:

$$X(t) = \frac{\int_0^{R_p} R^{Fp-1}\, x(R,t)\, dR}{\int_0^{R_p} R^{Fp-1}\, dR} \tag{35}$$

where Fp is the pellet shape factor and represents the power of the principle dimension when calculating pellet volume. (Fp = 1, 2, or 3 for disc, cylindrical or spherical pellets respectively.)

C. MULTI-REACTION MODEL

In this section, the single-reaction model is extended to accommodate the two-reaction system described by the simultaneous reactions given below:

Reaction 1:

$$A_{(g)}+B_{(s)} \longrightarrow 2C_{(g)} \qquad (36a)$$

Reaction 2:

$$D_{(s)}+C_{(g)} \longrightarrow E_{(s)}+A_{(g)} \qquad (36b)$$

For this system, two types of solid grains are present in the pellet: grains composed of solid B and grains composed of solid D. The solids are initially present with volume fractions of α_{Bo} and α_{Do}. Only gaseous reactant A is present in the bulk gas stream.

The development of the multi-reaction model is very similar to that of the single-reaction model. Consider, once again, the volume element of thickness ΔR at the position R in the pellet, as shown in Figure 2. For this system, a material balance on A results in

$$N_A S_E\big|_{R+\Delta R} - N_A S_E\big|_R - V_E S_{v1} f_1(C_{Ai1}, C_{Ci1}) + V_E S_{v2} f_2(C_{Ai2}, C_{Ci2}) = 0 \qquad (37)$$

The first and second terms refer to the amounts of A entering and leaving the volume element respectively. The third term in equation

(37) accounts for the consumption of A due to Reaction 1 in the element. $f_1(C_{Ai1}, C_{Ci1})$ is the intrinsic reaction rate per unit surface area for Reaction 1; C_{Ai1} and C_{Ci1} are the concentrations of A and C respectively at the reaction front inside the solid B grains. S_{v1} is the surface area in the pellet available for Reaction 1 to take place (per unit volume of pellet). This is expressed by:

$$S_{v1} = 3\alpha_{Bo} \frac{r_{cB}^2}{r_{oB}^3} \tag{38}$$

where r_{cB} is the radius of the reaction front in B grains and r_{oB} is the initial B grain radius.

The fourth term in equation (37) accounts for the production of A due to Reaction 2, where $f_2(C_{Ai2}, C_{Ci2})$ describes the intrinsic reaction kinetics of Reaction 2 and S_{v2} is found from:

$$S_{v2} = 3\alpha_{Do} \frac{r_{cD}^2}{r_{oD}^3} \tag{39}$$

Definitions for r_{cD}, r_{oD}, C_{Ai2} and C_{Ci2} are analagous to above.

The molar flux N_A is given by Equation (4). Assuming constant total concentration:

$$N_A = x_A(N_A + N_C) - D_{eA} \frac{dC_A}{dR} \tag{40}$$

Stoichiometry of the reaction dictates that, from Reaction 1:

$$N_C = -2N_A \tag{41}$$

and from Reaction 2:

$$N_C = - N_A \tag{42}$$

Therefore:

$$N_C = -3/2\ N_A \tag{43}$$

and:

$$N_A = - \frac{D_{eA}}{1+x_A/2} \frac{dC_A}{dR} \tag{44}$$

and equation (37) for the conservation of A becomes:

$$\frac{1}{1+x_A/2}\frac{\partial}{\partial R}\left(D_{eA}\frac{\partial C_A}{\partial R}\right) - 3\alpha_{Bo}\frac{r_{cB}^2}{r_{oB}^3} f_1(C_{Ai1},C_{Ci1}) + 3\alpha_{Do}\frac{r_{cD}^2}{r_{oD}^3} f_2(C_{Ai2},C_{Ci2}) = 0 \qquad (45)$$

A similar development results in the equation governing the conservation of C:

$$-\frac{1}{1-x_C/3}\frac{\partial}{\partial R}\left(D_{eC}\frac{\partial C_C}{\partial R}\right) + 6\alpha_{Bo}\frac{r_{cB}^2}{r_{oB}^3} f_1(C_{Ai1},C_{Ci1}) - 3\alpha_{Do}\frac{r_{cD}^2}{r_{oD}^3} f_2(C_{Ai2},C_{Ci2}) = 0 \qquad (46)$$

Since Reaction 1 (equation (36a)) leaves no solid product layer around the B grains, the concentrations of A and C at the reaction front in B grains are equal to the concentrations in the pores between the grains.

Thus:

$$C_{Ai1} = C_A \tag{47a}$$

$$C_{Ci1} = C_C \tag{47b}$$

However, the second reaction (equation (36b)) does leave a product layer around the D grains. Thus, to find C_{Ai2} and C_{Ci2}, the flux of A and C through this product layer must be considered. Fick's Law dictates that:

$$N_{A2} = -D_{gA2} \frac{dC_A}{dR} \tag{48}$$

or

$$\frac{dn_{A2}}{dt} = -4\pi r_{gD} r_{cD} D_{gA2} \frac{C_A - C_{Ai1}}{r_{gD} - r_{cD}} \tag{49}$$

where D_{gA2} is the diffusivity of A through the product layer surrounding D grains.

A similar expression can be developed for the flux of C through the product layer:

$$\frac{dn_{C2}}{dt} = - 4\pi\, r_{gD}\, r_{cD}\, D_{gC2}\, \frac{C_C - C_{Ci2}}{r_{gD} - r_{cD}} \tag{50}$$

From reaction kinetics, it is known that:

$$\frac{dn_{A2}}{dt} = 4\pi\, r_{cD}^{\,2}\, f_2(C_{Ai2}, C_{Ci2}) \tag{51}$$

and:

$$\frac{dn_{C2}}{dt} = -4\pi\, r_{cD}^{\,2}\, f_2(C_{Ai2}, C_{Ci2}) \tag{52}$$

Simultaneous solution of Equations (44) - (47) and (49) - (52) results in values for C_A, C_C, C_{Ai1}, C_{Ci1}, C_{Ai2}, C_{Ci2}, dn_{A2}/dt and dn_{C2}/dt.

Finally, the conservation equations for solid reactants B and D are derived. From the stoichiometry of Reaction 1 (equation (36a)), it is known that

$$\frac{dn_B}{dt} = \frac{dn_{A1}}{dt} \tag{53}$$

From reaction kinetics:

$$\frac{dn_{A1}}{dt} = -4\pi r_{cB}^{2} f_1(C_{Ai1}, C_{Ci1}) \tag{54}$$

Following the development of the single reaction model, the conservation equations for the solid reactant B becomes:

$$\rho_B \frac{dr_B}{dt} = -f_1(C_{Ai1}, C_{Ci1}) \tag{55}$$

From the stoichiometry for Reaction 2 (equation (36b)),

$$\frac{dn_D}{dt} = \frac{dn_{C2}}{dt} \tag{56}$$

Following the same development as above, with an expression for dn_{C2}/dt provided by equation (52) the conservation of solid reactant D can be expressed as:

$$\rho_D \frac{dr_D}{dt} = -f_2(C_{Ai2}, C_{Ci2}) \tag{57}$$

In general, the grain radii, r_{gB} and r_{gD}, change as the reaction proceeds. Since there is no product layer around B grains, the grain radius will equal the reaction front radius:

$$r_{gB} = r_{cB} \tag{58}$$

For D grains, the grain radius is determined by a material balance on the product layer surrounding D grains. For spherical grains,

$$(r_{gD}^3 - r_{cD}^3) \frac{\rho_E}{M_E} (1 - \varepsilon_E) = (r_{oD}^3 - r_{cD}^3) \frac{\rho_D}{M_D} \tag{59}$$

where ε_E is the porosity of the product layer.

The changes in the grain radii affect the porosity of the pellet according to equation (60):

$$\varepsilon = 1 - \alpha_B - \alpha_D \tag{60}$$

where α_B and α_D are found from equations (61) and (62):

$$\frac{\alpha_B}{\alpha_{Bo}} = \frac{r_{gB}^3}{r_{oB}^3} \tag{61}$$

$$\frac{\alpha_D}{\alpha_{Do}} = \frac{r_{gD}^3}{r_{oD}^3} \tag{62}$$

These equations are developed in a similar manner to equation (29) for the single-reaction model.

The effective diffusivity is affected by the changing porosity according to the random pore model [79]:

$$D_e = D\varepsilon^2 \tag{63}$$

The initial and boundary conditions for the multi-reaction model are as follows:

(1) There is no reaction before time t = 0. Thus, for all R,

$$r_{cB} = r_{oB} \text{ at } t = 0 \tag{64a}$$

$$r_{cD} = r_{oD} \text{ at } t = 0 \tag{64b}$$

(2) There is symmetry at the center of the pellet:

$$\frac{\partial C_A}{\partial R} = 0 \quad \text{at } R = 0 \tag{65a}$$

$$\frac{\partial C_C}{\partial R} = 0 \quad \text{at } R = 0 \tag{65b}$$

3) The diffusive flux into the pellet equals the convective flux across the external gas film:

$$\frac{D_{eA}}{1+x_A/2}\frac{\partial C_A}{\partial R} = h(C_{Ab}-C_A) \qquad \text{at } R = R_p \tag{66a}$$

$$\frac{D_{eC}}{1-x_C/3}\frac{\partial C_C}{\partial R} = h(C_{Cb}-C_C) \qquad \text{at } R = R_p \tag{66b}$$

The local conversion of the solid reactants B and D are found by comparing the reaction front radii at any time to the initial grain radii:

$$x_B(R,t) = 1 - \frac{r_{cB}(R,t)^3}{r_{oB}^3} \tag{67}$$

$$x_D(R,t) = 1 - \frac{r_{cD}(R,t)^3}{r_{oD}^3} \tag{68}$$

The local conversions are converted to individual overall (or global)conversions by summing across the pellet.

$$X_B(t) = \frac{\int_0^{R_p} R^{Fp-1} \, x_B(R,t) \, dR}{\int_0^{R_p} R^{Fp-1} \, dR} \tag{69}$$

$$X_D(t) = \frac{\int_0^{R_p} R^{Fp-1} \, x_D(R,t) \, dR}{\int_0^{R_p} R^{Fp-1} \, dR} \tag{70}$$

Total pellet conversion is found by calculating the ratio of pellet weight loss at time to the total possible pellet weight loss:

$$X_T = \frac{(M_D - M_E)X_D\gamma + M_B X_B}{(M_D - M_E)\gamma + M_B} \tag{71}$$

where γ is the molar ratios of D to B in the pellet.

D. AUXILIARY EQUATIONS

In this section, the equations used to calculate the effective diffusivities of A and C and the external mass transfer coefficient are presented. The majority of these equations are well established in

literature. References are provided for more complete discussions of the equations presented here.

1. Effective Diffusivities of A and C

Rothfield and Watson [80] derived an expression for the composite diffusivity of gas A for the binary pair A-C at steady state. In this case,

$$\frac{1}{D_A} = \frac{1}{D_{KA}} + \frac{1}{D_{AC}}\left[\frac{N_A/(-N_C)-1}{\ln(N_A/(-N_C))}\right] \tag{72}$$

where D_{AC} is the molecular diffusivity of the binary pair A-C and D_{KA} is the Knudsen diffusivity of A.

The molecular diffusivity D_{AC} is determined from the Chapman-Enskog kinetic theory [81] as:

$$D_{AC} = 0.001853 \frac{\left[T^3(1/M_A+1/M_C)\right]^{\frac{1}{2}}}{P\,\sigma_{AC}^{\,3}\,\Omega_{D,AC}} \tag{73}$$

where

D_{AC} = molecular diffusivity, cm^2/s

T = temperature, K

M_A, M_C = molecular weights of A and C, g/mol

P = pressure, atm

σ_{AB} = constant in the Lennard-Jones 12-6 potential function, A.Table B-1 of [81] gives values of σ_A and σ_C. σ_{AC} is found from

$$\sigma_{AC} = \tfrac{1}{2}(\sigma_A + \sigma_C) \tag{74}$$

$\Omega_{D,AC}$ = dimensionless function of temperature and intermolecular potential field for one molecule of A and one molecule of C. Table B-2 of [81] gives $\Omega_{D,AC}$ as a function of kT/ε_{AC} where:

$$\frac{\varepsilon_{AC}}{k} = \left(\frac{\varepsilon_A}{k}\frac{\varepsilon_C}{k}\right)^{\frac{1}{2}} \tag{75}$$

ε_A/k and ε_C/k are constants in the Lennard-Jones 12-6 potential function and are given in Table B-1 of [81].

The Knudsen diffusivity of A is given by [82]

$$D_{KA} = \frac{d_p}{3}\left(\frac{8RT}{\pi M_A}\right)^{\frac{1}{2}} \tag{76}$$

where d_p is the characteristic pore dimension. For closely-packed, spherical grains of initial radius r_o and radius at any time r_g, the volume of the pore space per grain P_V is given by:

$$P_V = (2r_o)^3 - 4/3\pi r_g^3 \tag{77}$$

If the interstices between the grains are approximated to be of cubical shape, then the pore dimension d_p can be expressed as

$$d_p^3 = (2r_o)^3 - 4/3\pi r_g^3 \tag{78}$$

A similar scheme as above is used to calculate the effective diffusivities of A and C in the product layer surrounding individual grains. In order to do these calculations, however, it is necessary to know the porosity and characteristic pore dimension in the product layer. As no values are given for these properties in the experimental data, they have to be approximated. The value of the porosity in the product layer ε_D is assumed to be constant throughout the product layer. With an assumed value of ε_D*, the pore dimension, d_{pg}, is found from the ratio of product layer porosity and intergranular porosity:

$$d_{pg} = d_p \frac{\varepsilon_D}{\varepsilon} \tag{79}$$

---

* It was found that the value of ε_D had negligible effect on the results generated by the models. A value of 0.05 was used for all runs.

where d_p and ε are the values of intergranular pore dimension and porosity.

With these values of ε_D and d_{pg}, the effective diffusivities of A and C in the product layer can be calculated from equations (72), (73), (76) and (78).

2) External Mass Transfer Coefficient

The external mass transfer coefficient h is calculated from well-established correlations. For spherical pellets with Reynolds number in the range of 20 to 2000, Rowe and Claxton [83] propose the following correlation:

$$Sh = 2.0 + 0.69\ Re^{1/2}\ Sc^{1/3} \tag{80}$$

For flow perpendicular to cylinders, the following correlation applies:

$$Sh = (0.35 + 0.34\ Re^{0.5} + 0.15\ Re^{0.58})\ Sc^{0.3} \tag{81}$$

for $0.1 < Re < 10^5$ and $0.7 < S_c < 1500$. Finally, for flow parallel to flat plates [82],

$$Sh = 0.664\ Re^{1/2}\ Sc^{1/3} \tag{82}$$

when $Re < 50{,}000$

Both Re and Sc depend on the viscosity of the bulk gas stream. This is calculated using the method of Thodos [84].

$$\mu\xi = 4.610\ T_r^{0.618} - 2.04\ e^{-0.449T_r} + 1.94\ e^{-4.058T_r} + 0.1 \tag{83}$$

where μ is the viscosity (micropoise) and

$$\xi = T_c^{1/6}\ M^{-1/2}\ P_c^{-2/3} \tag{84}$$

T_c, M and P_c are properties of the bulk gas stream. In this study, the bulk gas streams were pure gas; therefore no mixing rules were required.

Density of the bulk gas stream is calculated from the ideal gas law, as system pressures in this study are atmospheric.

IV NUMERICAL SOLUTION OF THE MODELS

Due to the complexity of the model equations, the models cannot be solved analytically; they must be solved numerically. The methods of solution for both the single-reaction model and the multi- reaction model are very similar. For this reason, only the solution of the single-reaction model will be discussed in detail. Comments will be made where the multi-reaction model differs.

The solution of the model is achieved by establishing a grid system which divides the pellet radius R_p into n grid spaces with m(= n+1) nodes i. Node i = 1 is the centre of the pellet (R = 0) and node i = m is the pellet surface ($R = R_p$). Model equations containing differentials with respect to space are discretized using this grid system. This includes the conservation equations for the gaseous components A and C. (equations (10) and (15) for the single-reaction model and equations (44) and (45) for the multi- reaction model.)

Second order differentials are discretized using a second order central difference formula. For example,

$$\frac{d^2C_A}{dR^2} = \frac{1}{h^2}\left[C_A(i-1) - 2C_A(i) + C_A(i+1)\right] + O(h^2) \qquad (85)$$

where

$$h = R_p/n \tag{86}$$

First order differentials at interior points are discretized using a first order central difference formula as follows:

$$\frac{dC_A}{dR} = \frac{1}{2h}\left[-C_A(i-1) + C_A(i+1)\right] + O(h^2) \tag{87}$$

At the pellet exterior ($R = R_p$) and the pellet center ($R = 0$) the first order differential is discretized, using second order backward and forward difference equations respectively:

$$\left.\frac{dC_A}{dR}\right|_{R=R_p} = \frac{1}{2h}\left[C_A(i-2) - 4C_A(i-1) + 3C_A(i)\right] + O(h^2) \tag{88}$$

$$\left.\frac{dC_A}{dR}\right|_{R=0} = \frac{1}{2h}\left[-3C_A(i) + 4C_A(i+1) - C_A(i+2)\right] + O(h^2) \tag{89}$$

All properties in the pellet are given discrete values at each node. Each model equation is written at each node.

The algorithm given in Figure 3 is used to solve the model. To begin the solution, the physical constants of the system are input or calculated. Initial structural properties are input, as well as

reaction system constants. These are used to calculate diffusivities and the external mass transfer coefficient. The initial conditions are then set appropriately. The grain radius and effective diffusivities of A and C are calculated by subroutine PROPS.

Subroutine PROFILE is then called to calculate the initial concentration profiles in the pellet. The subroutine simultaneously solves equations (9), (15), (18) - (21) (equations (44), (47) and (49) - (52) in the multi-reaction model) at each node i for the unknowns $C_A(i)$, $C_c(i)$, $C_{Ai}(i)$, $C_{ci}(i)$, $dn_A(i)/dt$, $dn_C(i)/dt$.

A starting guess is supplied and the equations are solved simultaneously using a Gauss-Siedel iterative scheme.

Once the concentration profiles are known, the time is advanced by one time step and updated values of the reaction front radii at each node are calculated. For this purpose, subroutine TSTEP is called. In this subroutine, the conservation equation for solid reactant B is solved. The solution of this equation is accomplished by using a fourth order Runge-Kutta technique using concentration profiles from the previous time step. In the multi-reaction model, TSTEP solves the conservation equations for solids B and D independently, using a fourth order Runge-Kutta technique.

Once the updated reaction front radii are calculated, subroutine CONVER is called to calculate the conversion. The local conversion at

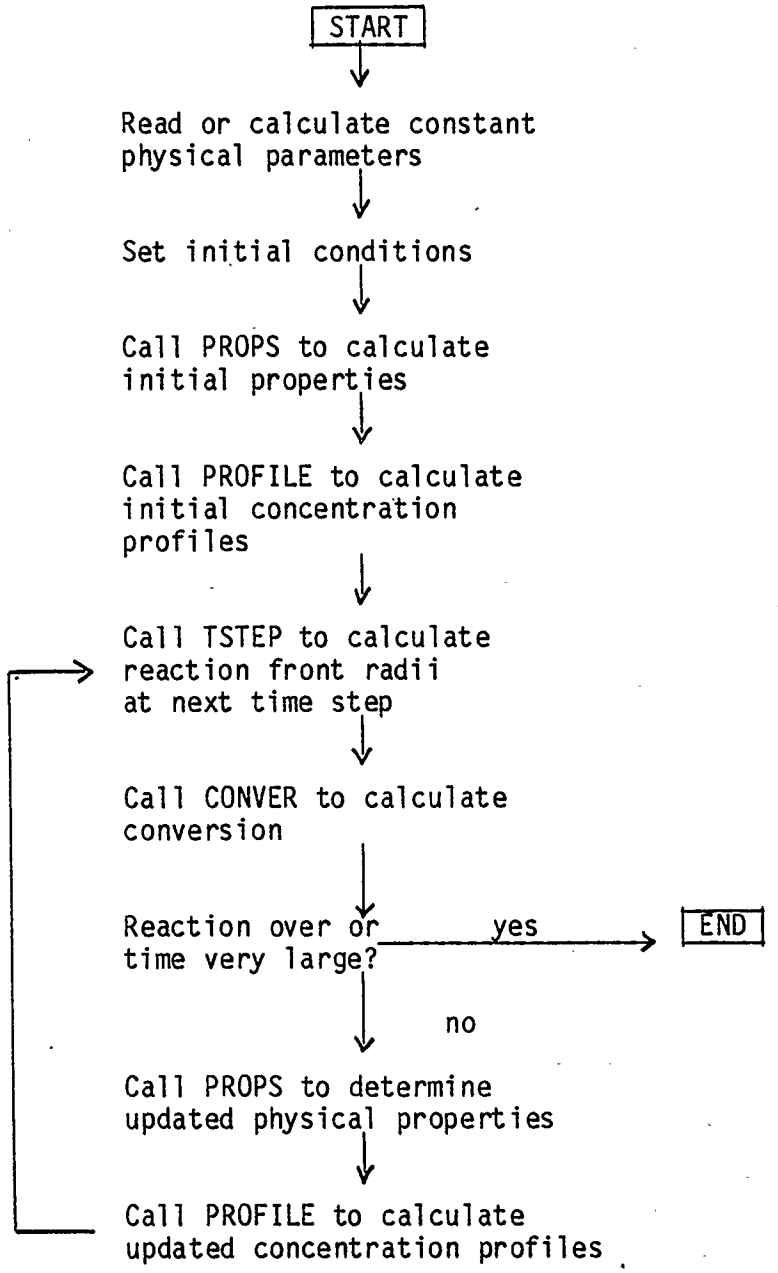

Figure 3 - NUMERICAL SOLUTION ALGORITHM

each node is calculated using the reaction front radii and equation (34) (equations (67) and (68) for the multi-reaction model). The global conversion is found by numerically integrating equation (35) using a Simpson's composite method. (Global conversions for the two reactant solids in the multi-reaction model are found independently by numerically integrating equations (69) and (70). Total pellet conversion is found from equation (71)).

If the conversion is complete or the time exceeds a set limit, the program is terminated. Otherwise, updated physical properties are calculated using subroutine PROPS. Subroutine PROFILE is recalled to update the concentration profiles. The program then returns to the point where the time is increased by one time step; the procedure from that point is repeated.

Output from the algorithm is generated at each time step and includes:

1) total conversion

2) concentration profiles for A and C

3) grain radii and reaction front radii profiles

4) diffusivity profiles.

V EXPERIMENTAL STUDIES

To test the models derived in this study, the model predictions were compared to experimental results. All experimental results used for comparison are those of Hastaoglu [65]. In order to facilitate the understanding of the comparisons, a brief explanation of the experimental apparatus and procedure used to generate the results are presented here.

Figure 4 shows a schematic diagram of the experimental apparatus. The solid reactant powder is pressed into a disc-shaped pellet (Fp = 1, diameter = 2.86 cm, thickness varies with experimental run). The pellet is placed in reaction basket and is placed into the upper section of the reaction tube (ID = 2 inches). In this section, no reaction takes place. The entire system (upper and lower sections) is flushed with an inert gas, such as nitrogen or helium.

The lower reaction zone is isolated from the upper zone by a gate valve. The reaction zone is surrounded by a furnace which heats the zone to the desired reaction temperature. When this zone is preheated, the reactant gas is allowed to flow through the reaction zone at the desired flow rate. The gate valve is opened and the solid pellet is lowered into the heated reaction zone. The reaction begins and the weight change of the pellet is measured and recorded automatically. A more complete description of the experimental system is given by Hastaoglu [65].

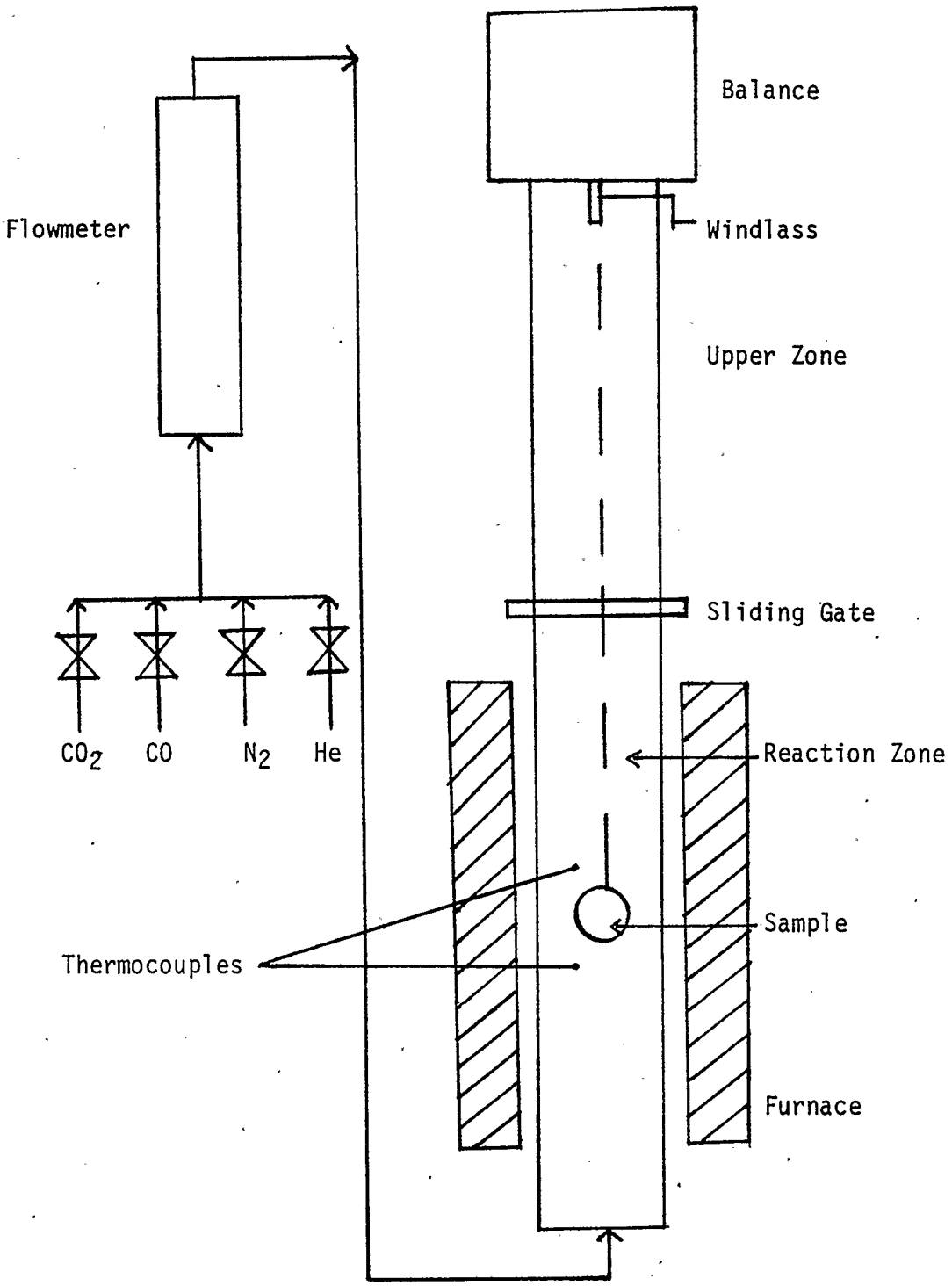

Figure 4 Schematic of Experimental Apparatus

VI RESULTS

A. INTRODUCTION

The single-reaction model was tested by comparing model predictions to experimental data for each of three systems. These include:

1) Noncatalytic carbon gasification

2) Catalytic carbon gasification

3) Nickel oxide reduction

The multi-reaction model was tested with the nickel oxide/carbon/carbon dioxide system. For each of these systems, the model predictions were compared to the experimental work of Hastaoglu [65].

B. CARBON GASIFICATION

1) Noncatalytic Carbon Gasification

The single-reaction model was first tested by attempting to predict noncatalytic gasification of carbon black with carbon dioxide. The reaction is described by the following equation:

$$C + CO_2 \longrightarrow 2\ CO$$

It is generally agreed in the literature that the kinetics of the above reaction can be modelled using a Langmuir-Hinshelwood rate equation:

$$\text{Rate} = \frac{k_1 P_{CO_2}}{1 + k_2 P_{CO} + k_3 P_{CO_2}}$$

In terms of concentration, this can be rewritten as

$$\text{Rate} = \frac{k_1 C_{CO_2}}{1/R_g T + k_2 C_{CO} + k_3 C_{CO_2}}$$

where C_{CO_2} and C_{CO} are the concentractions of reactant and product gases respectively at the reaction front.

Values for k_2 and k_3 were taken from Wu [85], who reports that for the mechanism of Gadsby et al [58]:

$$k_2 = 3.3 \times 10^{-9} \exp(60.50/R_g T) \quad atm^{-1}$$

$$k_3 = 0.1766 \exp(6.63/R_g T) \quad atm^{-1}$$

where the activation energies are reported in kcal/gmol.

The value of k_1 was found for each run by fitting the model predictions to the experimental data. It was assumed that k_1 is constant for each temperature (ie a single value of k_1 was used for the entire conversion range). In addition, k_1 was the only parameter used to fit the model to the experimental data. All other structural properties and reaction system properties were fixed for any given run. Appendix I contains the values of the experimental parameters used.

The single-reaction model was used to predict the conversion - time behaviour of the noncatalytic carbon gasification system at five temperatures between 800°C and 1100°C. Comparisons of the experimental behaviour and the model predictions are given in Figures 5 and 6. It can be seen that the model predictions are generally in excellent agreement with the experimental results.

At 1100°C, the model predicts the experimental results up to a conversion of 75%, with a maximum error of 10% at the lower conversions. At 1000°C, the match of model to experimental results is excellent, with negligible error.

At lower temperatures, experimental results indicate that an exposure time is required before reaction gets fully underway. At 800°C and 850°C, this is apparent as no reaction took place before one to two hours of exposure to the reactant gas. The model, as it is written, cannot account for such an exposure time. In order to

account for this occurrence at 800°C and 850°C, the model predictions were shifted so that reaction time t = 0 coincided with the time of the start of the reaction during the experiments. Once this shift was accomplished, the model predicted the conversion - time behaviour with excellent results.

At 900°C, the model prediction does not match the experimental results with a high degree of success. It seems reasonable that, although the reaction does actually start at time t = 0, the reaction does not become fully developed immediately (ie an exposure time is again needed before the reaction becomes fully developed). Because of the inability of the model to account for exposure time, it does not predict the experimental behaviour as well at 900°C as it did at the other temperatures.

Table 1 presents the values of k_1 at each temperature, found by fitting the model predictions to the experimental results.

Table 1 Rate Constant k_1 for Noncatalytic Carbon Gasification

T(°C)	$k_1 \times 10^8$ mol/atm m^2 s
800	0.65
850	5.00
900	6.50
1000	60.00
1100	290.00

During the fitting process, varying k_1 affected only the slope of the model curve and did not affect the trend predicted by the model. Thus, the fact that the shape of the model predictions are similar to the shape of the experimental behaviour (except for the exposure time) indicates that the model is a good one.

The reaction constant k_1 is considered to be an Arrhenius function of temperature. An Arrhenius plot of k_1 is shown in Figure 7. It can be seen that the fit is good. Analysis of the plot results in an activation energy of 56.98 kcal/gmol. Thus k_1 can be expressed as:

$$k_1 = 3.5112 \times 10^3 \exp(-56.98/R_g T) \quad \text{mol/atm m}^2\text{s}$$

In Table 2, the value of activation energy from this study is compared to literature values.

Table 2 Comparision of Activation Energy for Noncatalytic Carbon Gasification

T range (°C)	Material	ΔE (kcal/mole)	Reference
890 - 1098	Carbon black	59	86
839 - 1050	Carbon black	79.6	61
700 - 1400	Graphite	59	59
817 - 1058	New England Coke	67.8	85
871 - 1085	Electrode Carbon	56.6	85
802 - 1093	New England Coke	54.3	87
700 - 830	Coconut Shell Charcoal	58.8	58
677 - 817	Carbon black	67.0	62
716 - 986	Carbon black	61.4	63
735 - 942	Carbon black	55.8	63
800 - 1000	lignite char	33.5	64
800 - 1100	Carbon black	57.0	present study

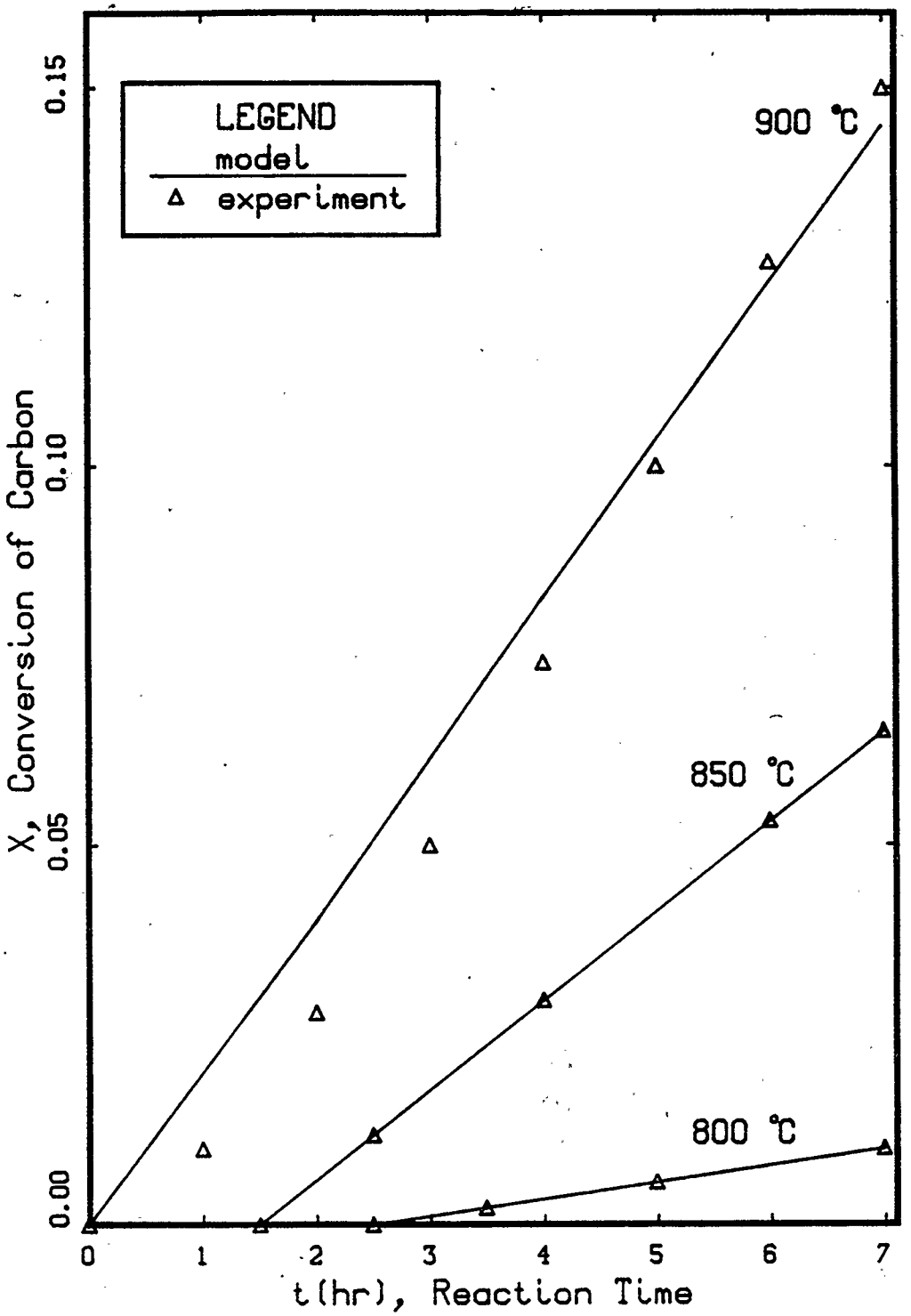

Figure 5 Conversion vs time, noncatalytic carbon gasification

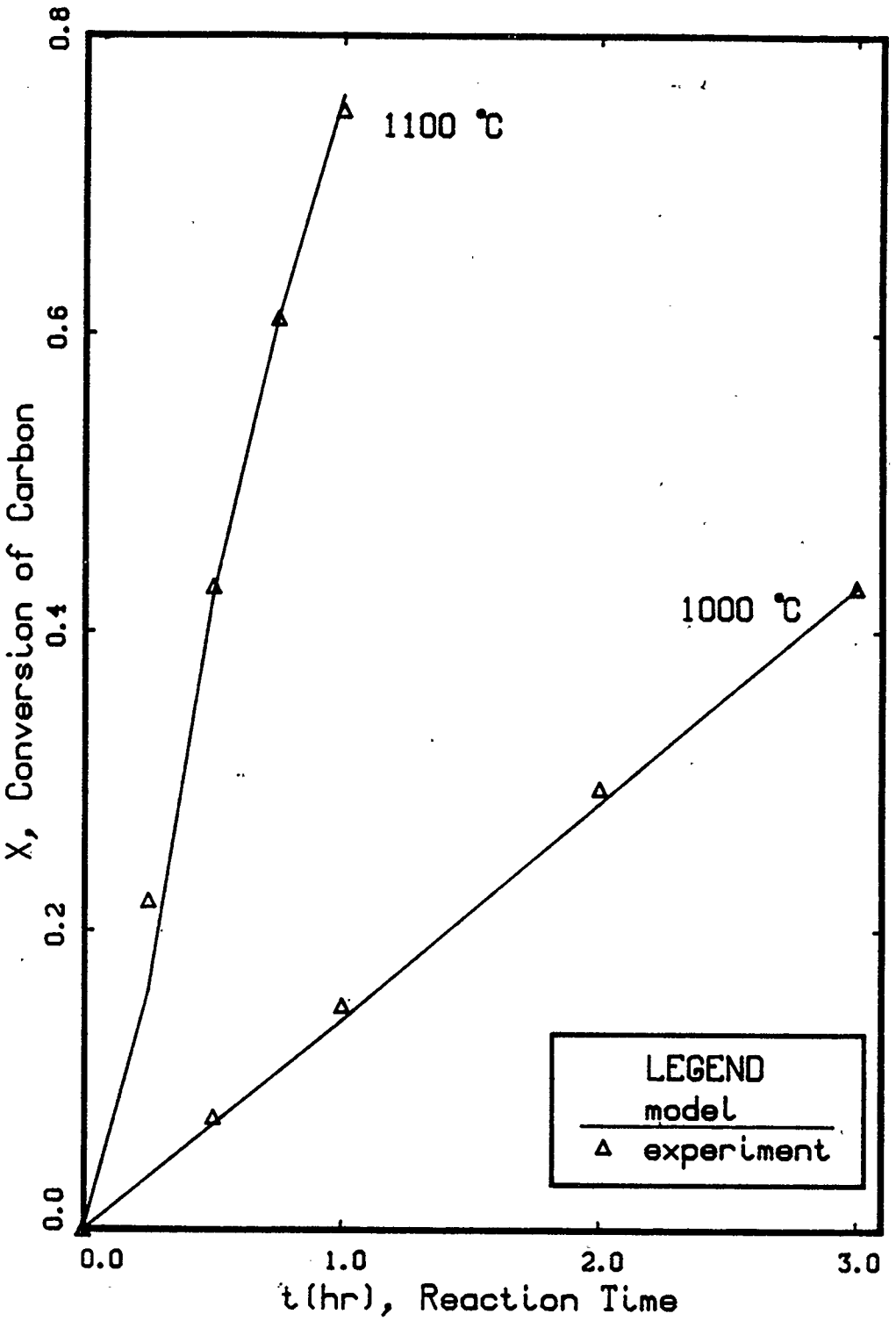

Figure 6 Conversion vs time, noncatalytic carbon gasification

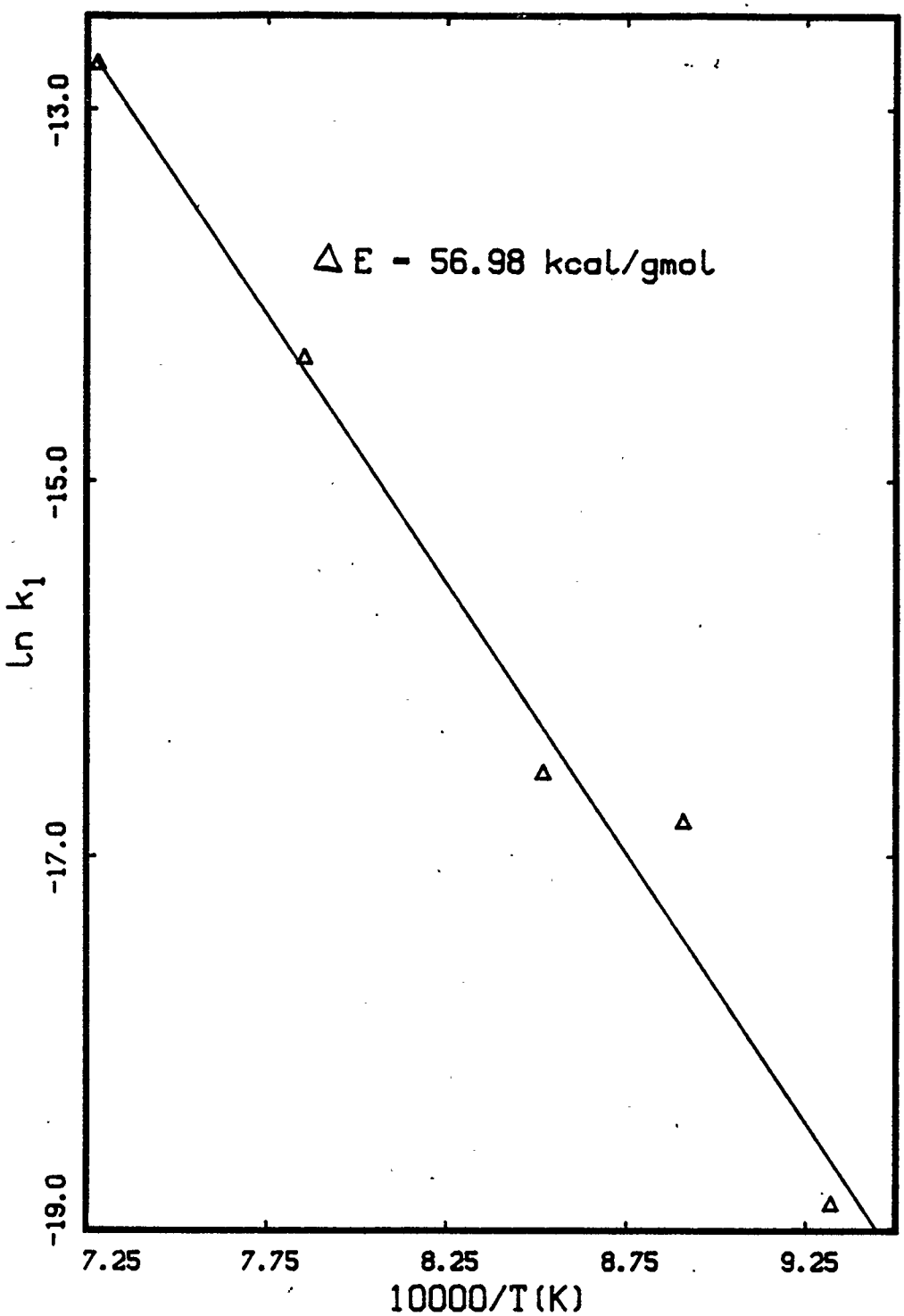

Figure 7 Arrhenius plot for rate constant k_1 for carbon gasification

The activation energy from this study falls in the range of those reported in the literature. This agreement indicates that the single-reaction model works well in predicting noncatalytic carbon gasification.

2) Catalytic Carbon Gasification

The single-reaction model was also tested with carbon gasification which is catalyzed due to the presence of nickel in the pellet. The reaction is described by the following equation:

$$C + CO_2 + Ni \longrightarrow 2CO + Ni$$

The reaction was modelled using a Langmuir-Hinshelwood type of kinetics, similar to the kinetics for the noncatalytic carbon gasification system. In this case, an additional term is added to incorporate the catalytic effect. The rate is described by the following equation:

$$\text{Rate} = \frac{(k_1 + k_c \rho_{Niapp}) P_{CO_2}}{1 + k_2 P_{CO} + k_3 P_{CO_2}}$$

where k_c is called the catalytic rate constant and ρ_{Niapp} is the apparent nickel density in the pellet. Derivation of the equation is given by Hastaoglu [65].

Because of the lack of data available for rate constants for catalytic carbon gasification, k_2 and k_3 for the noncatalytic carbon gasification system were used:

$$k_2 = 3.3 \times 10^{-9} \exp[60593/R_gT] \quad atm^{-1}$$

$$k_3 = 0.1766 \exp [6626/R_gT] \quad atm^{-1}$$

where R_g = 1.987 cal/gmol K. Values for k_1 were taken from the results of the noncatalytic carbon gasification system, reported in the previous section. The values of k_1 which were found to best fit the experimental results at each temperature are repeated in Table 3 below.

Table 3 Values of Reaction Constant k_1 for use in the Catalytic Rate Equation

T(°C)	$k_1 \times 10^8$ mol/atm m^2s
800	0.65
850	5.00
900	6.50
1000	60.00
1100	290.00

For the catalytic carbon gasification system, Hàstaoglu ran experiments at four temperatures between 800°C and 1000°C. At each temperature, several experiments were run using increasing amounts of nickel catalyst in the pellet. The molar ratios of nickel in the pellet, γ, ranged from 0.05 to 1.0 mole of nickel per mole of carbon.

The catalytic rate constant k_c was used to fit the model predictions to the experimental data for each of these runs. All other

experimental parameters were fixed for a given run. Appendix 2 contains the experimental data for the catalytic carbon gasification system.

The value of ρ_{Niapp} (apparent nickel density) was found [65] by taking the ratio of the weight of nickel in the pellet to the total pellet volume. Thus ρ_{Niapp} is a function of molar ratio γ . The values of ρ_{Niapp} are given in Appendix 2.

Comparisons of the model predictions and the experimental results are shown in Figures 8 to 16. The model predicts the experimental results very well. The problem of modelling exposure time is again evident, particularly at the lower temperatures. To overcome this difficulty, the model was used to match the linear, more developed portions of the experimental results. This was done at 800°C and 850°C for all ranges of γ because, at these temperatures, the reactions clearly exhibit the phenomenon of exposure time.

At 900°C and 1000°C the reactions did start at time t = 0. Therefore no adjustments of the model predictions were made at these temperatures. However, as in the noncatalytic system, it is reasonable to suggest that there is still an induction effect whereby the reaction does not become fully developed until an exposure time is passed. The effect is greatest at 900°C and low molar ratios of nickel (ie low catalyst concentration). Conversely, the effect is minimal at 1000°C and high γ (ie high catalyst concentration).

Table 4 shows the values of the "best-fit" k_c for each experimental run. In the formulation of the rate expression for catalytic carbon gasification, it is assumed the k_c is only a function of temperature and is independent of the amount of catalyst present in the pellet. The effect of the amount of catalyst is taken into account by including the nickel density ρ_{Niapp} in the rate expression.

However, examination of Table 4 causes speculation that the rate constant k_c is indeed a function of amount of catalyst present (i.e. at low temperatures, k_c decreases with γ and at high temperatures, k_c increases with γ). A possible explanation for this unexpected phenomenon considers the uniformity of the distribution of the catalyst in the pellet. At low concentrations of nickel, mixing of nickel and carbon in the pellet was probably uniform. At higher nickel concentrations, however, the nickel may have agglomerated into areas of higher than average nickel concentration. These areas might have experienced very rapid reaction at high temperatures (as shown by the especially high k_c values). At lower temperatures, the agglomerates may have interfered with diffusion which would have caused the values of k_c to be lower than expected.

Tables 5 to 8 show the values of $k_c \rho_{Niapp}$ for each molar ratio at each experimental temperature. Although at 800°C no trend can be concluded, at 900°C and 1000°C (and to some extent 850°C) there is a noticeable trend in the value of $k_c \rho_{Niapp}$. The rate of reaction due to catalyst, $k_c \rho_{Niapp}$, increases with increasing molar ratio of catalyst. Thus, at least up to molar ratios of 1.0 mole

of nickel per mole of carbon, increasing catalyst amount increases the rate of reaction. This effect could be used to predict optimal catalyst concentration for a reaction.

Table 4 Catalytic Rate Constant k_c for each Experimental Run

T(°C)	γ $\frac{\text{(moles Ni)}}{\text{(mole C)}}$	$k_c x 10^6$ mol/atm k_gs
800	0.05	650
	0.1	270
	0.2	175
	0.4	85
	0.6	80
850	0.05	1,050
	0.1	950
	0.2	500
900	0.1	100
	0.2	350
	0.4	400
	0.6	425
	0.8	1,100
1000	0.05	2,700
	0.2	1,700
	0.4	1,300
	0.6	1.300
	0.8	4,600
	1.0	10,000

Table 5 Catalytic Rate Effect, T = 800°C

γ $\left(\frac{\text{moles Ni}}{\text{mole C}}\right)$	$k_c \rho_{Ni\,app}$ x 10^6 mol/atm m^2s
0.05	2.119
0.1	1.688
0.2	1.914
0.4	1.518
0.6	1.758

Table 6 Catalytic Rate Effect, T = 850°C

γ $\left(\frac{\text{moles Ni}}{\text{mole C}}\right)$	$k_c \rho_{Ni\,app}$ x10^6 mol/atm m^2s
0.05	3.434
0.1	5.852
0.2	5.600

Table 7 Catalytic Rate Effect, T = 900°C

γ $\left(\frac{\text{moles Ni}}{\text{mole C}}\right)$	$k_c \rho_{Ni\,app}$ x10^6 mol/atm m^2s
0.1	3.115
0.2	3.864
0.4	7.204
0.6	9.537
0.8	26.983

Table 8 Catalytic Rate Effect, T = 1000°C

γ $\left(\frac{\text{moles Ni}}{\text{mole C}}\right)$	$k_c \rho_{Niapp} \times 10^6$ mol/atm $m^2 s$
0.05	8.667
0.2	18.615
0.4	23.725
0.6	28.730
0.8	113.758
1.0	281.000

The catalytic rate constant k_c is assumed to be an Arrhenius function of temperature.

In order to find k_c for each temperature, a weighted average was calculated by the following equation. Thus at any temperature:

$$k_c = \frac{\Sigma k_c \rho_{Niapp}^2}{\Sigma \rho_{Niapp}^2}$$

Table 9 shows the values of k_c for each temperature.

Table 9 Catalytic Rate Constant k_c as a Function of Reaction Temperature.

T(°C)	$k_c \times 10^4$ mol m/atm kg s
800	1.072
850	6.319
900	6.616
1000	51.040

An Arrhenius plot of k_c is shown in Figure 17. Linear regression analysis of the data yields an activation energy for k_c of 50.4 kcal/gmol. The equation governing k_c becomes

$$k_c = 2.321 \times 10^6 \exp(-50.4/R_g T) \quad \frac{\text{mol m}}{\text{atm kgs}}$$

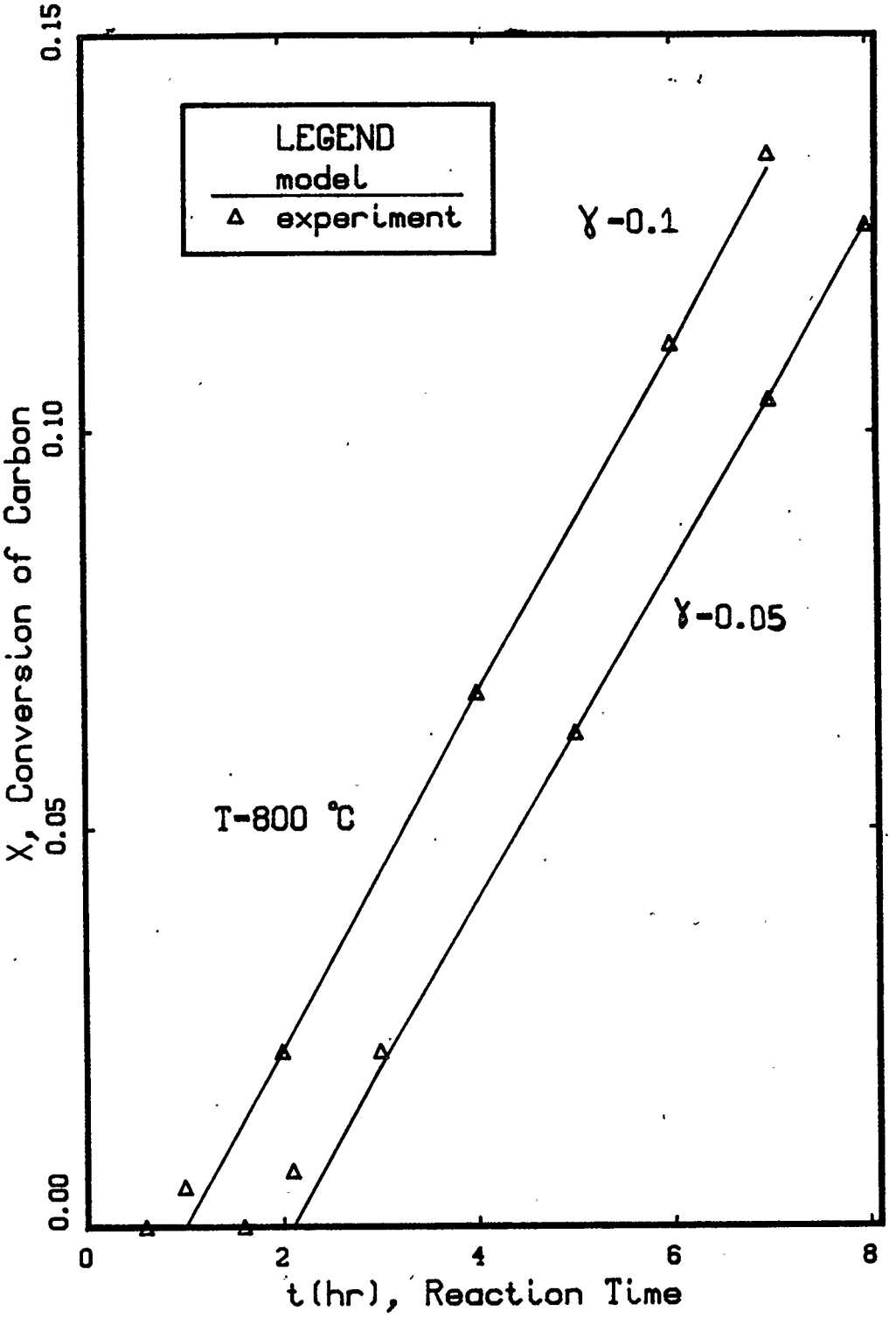

Figure 8 Conversion vs time, catalytic carbon gasification at 800 °C

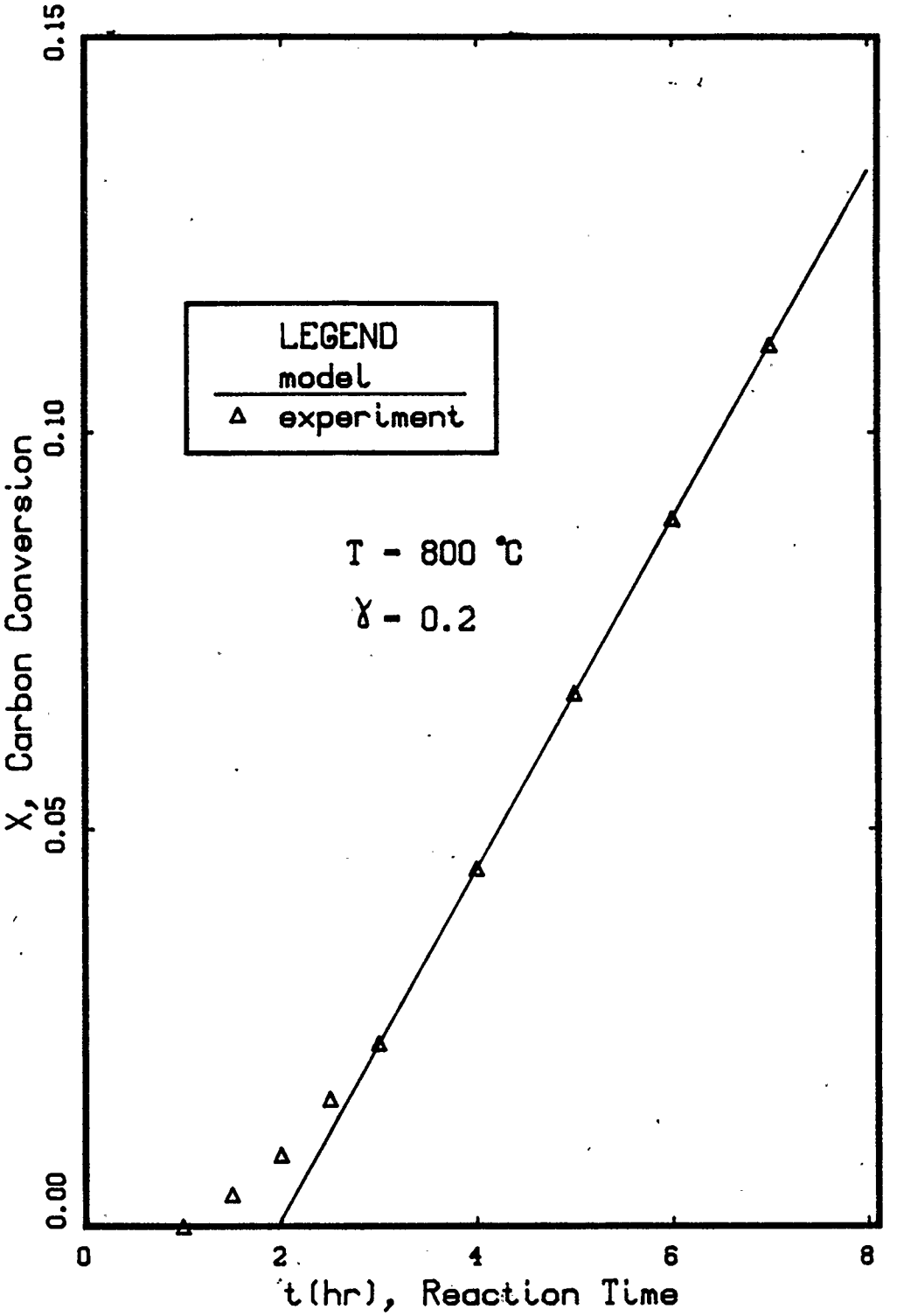

Figure 9 Conversion vs time, catalytic carbon gasification; T - 800 °C

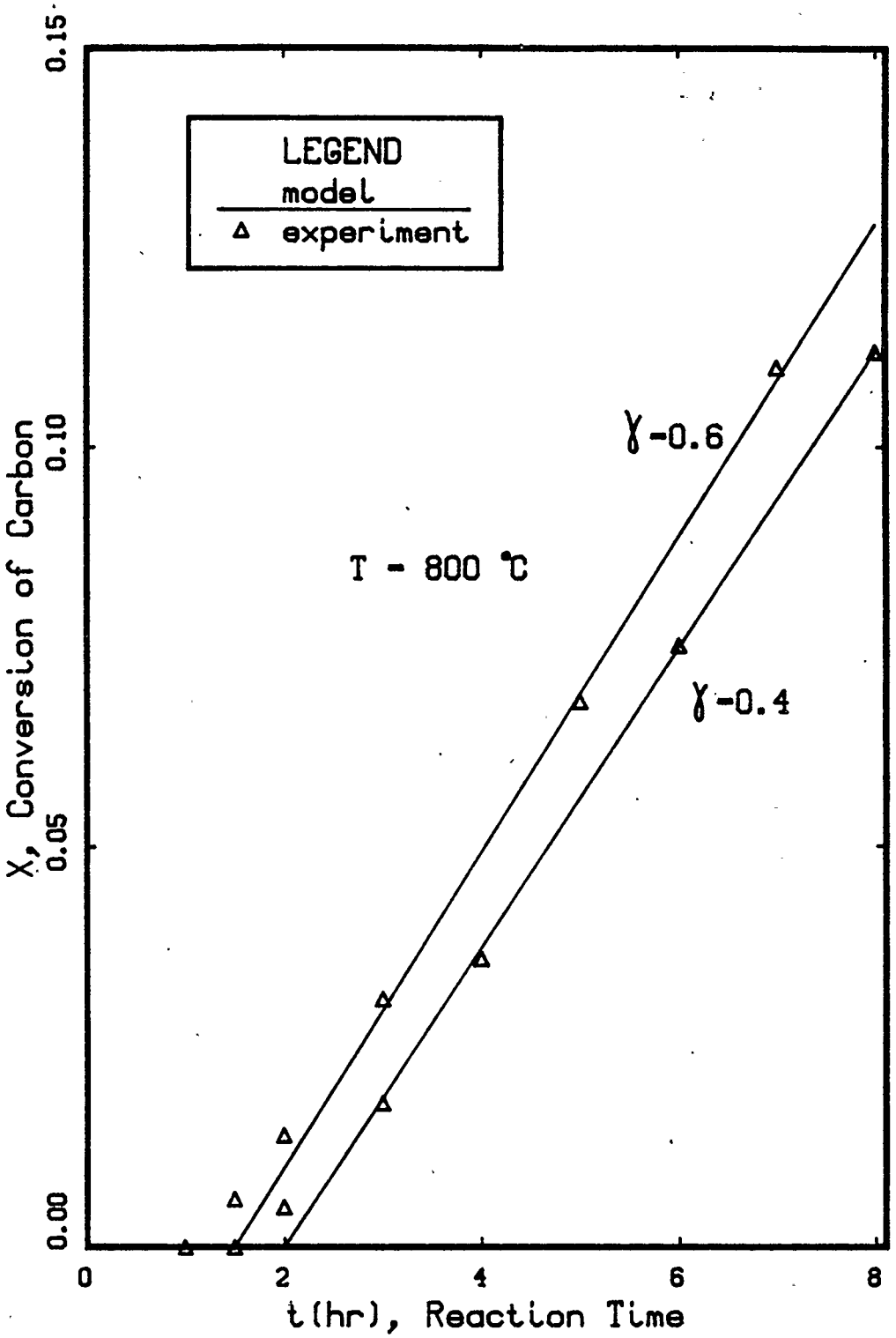

Figure 10 Conversion vs time, catalytic carbon gasification at 800 °C

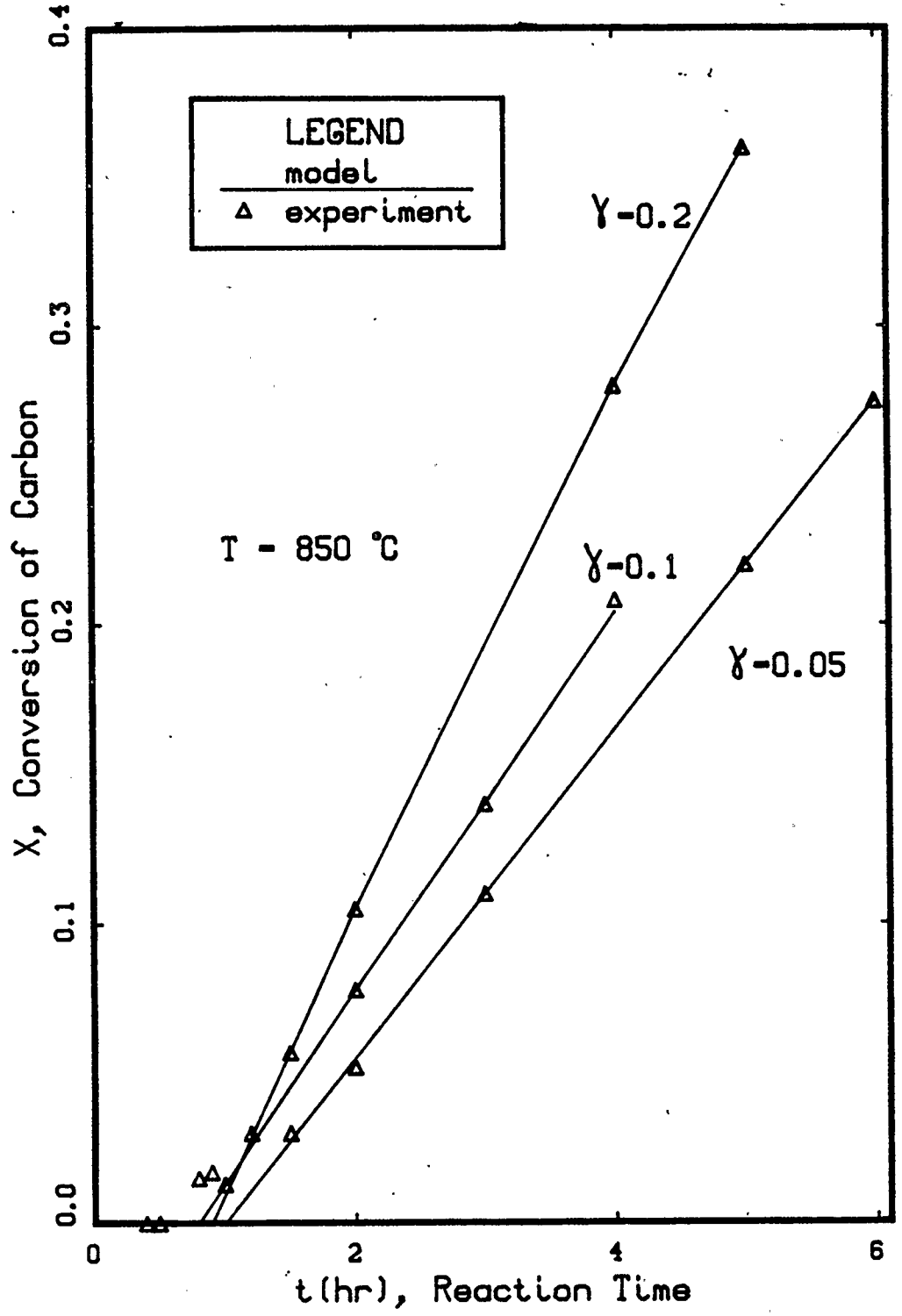

Figure 11 Conversion vs time, catalytic carbon gasification at 850 °C

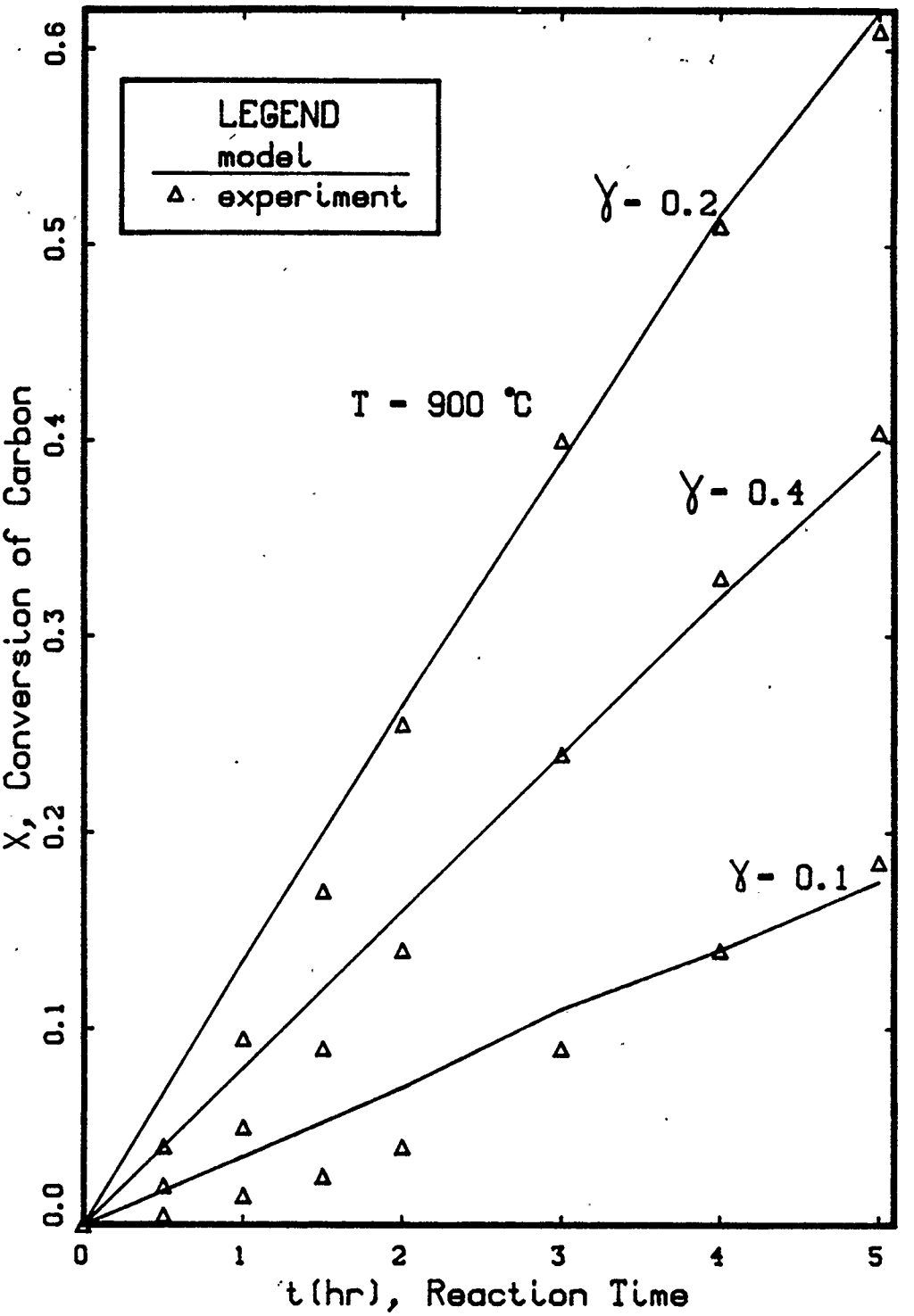

Figure 12 Conversion vs time, catalytic carbon gasification, T-900 °C

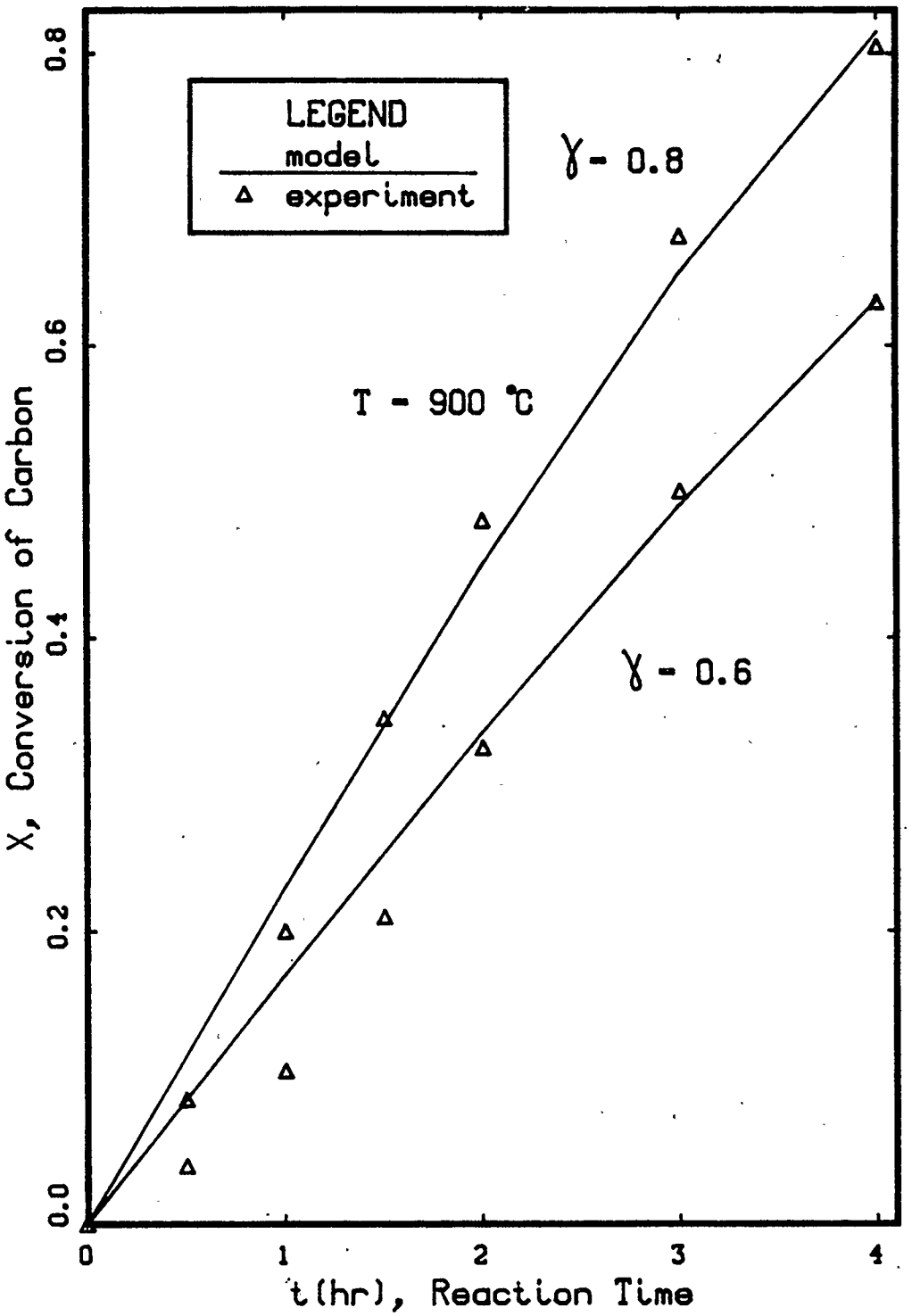

Figure 13 Conversion vs time, catalytic carbon gasification, T-900 °C

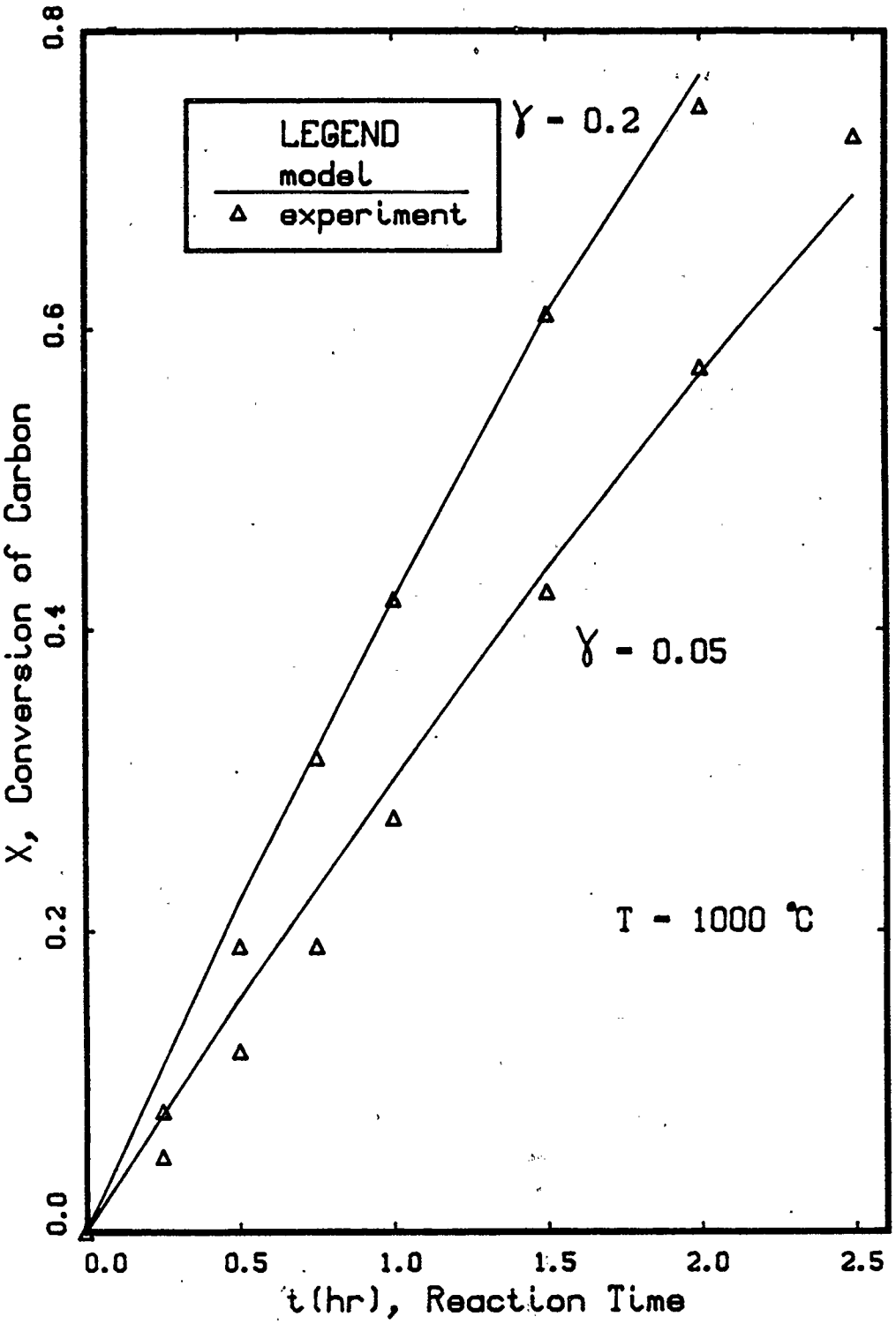

Figure 14 Conversion vs time, catalytic carbon gasification, T=1000 °C

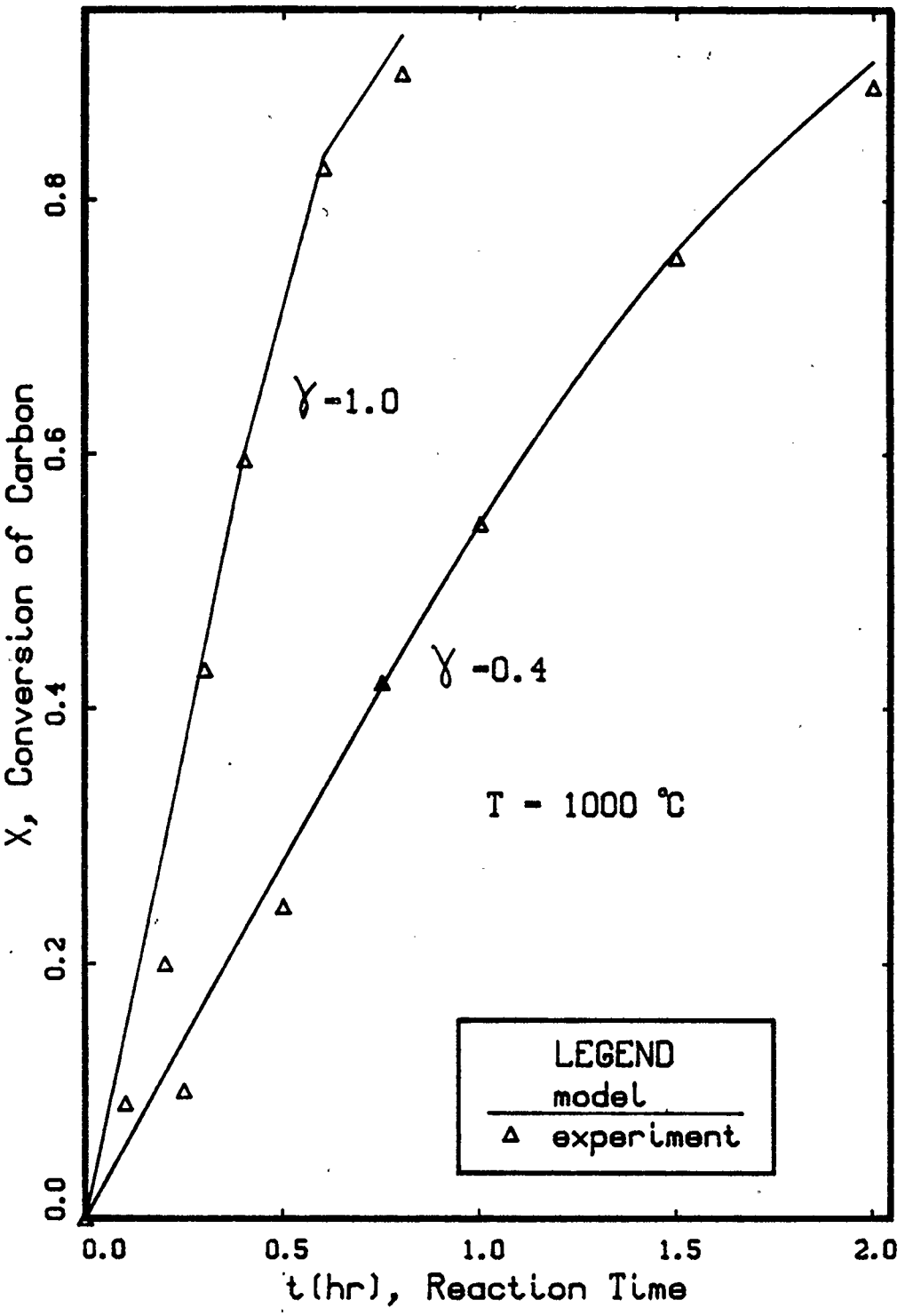

Figure 15 Conversion vs time, catalytic carbon gasification at 1000 °C

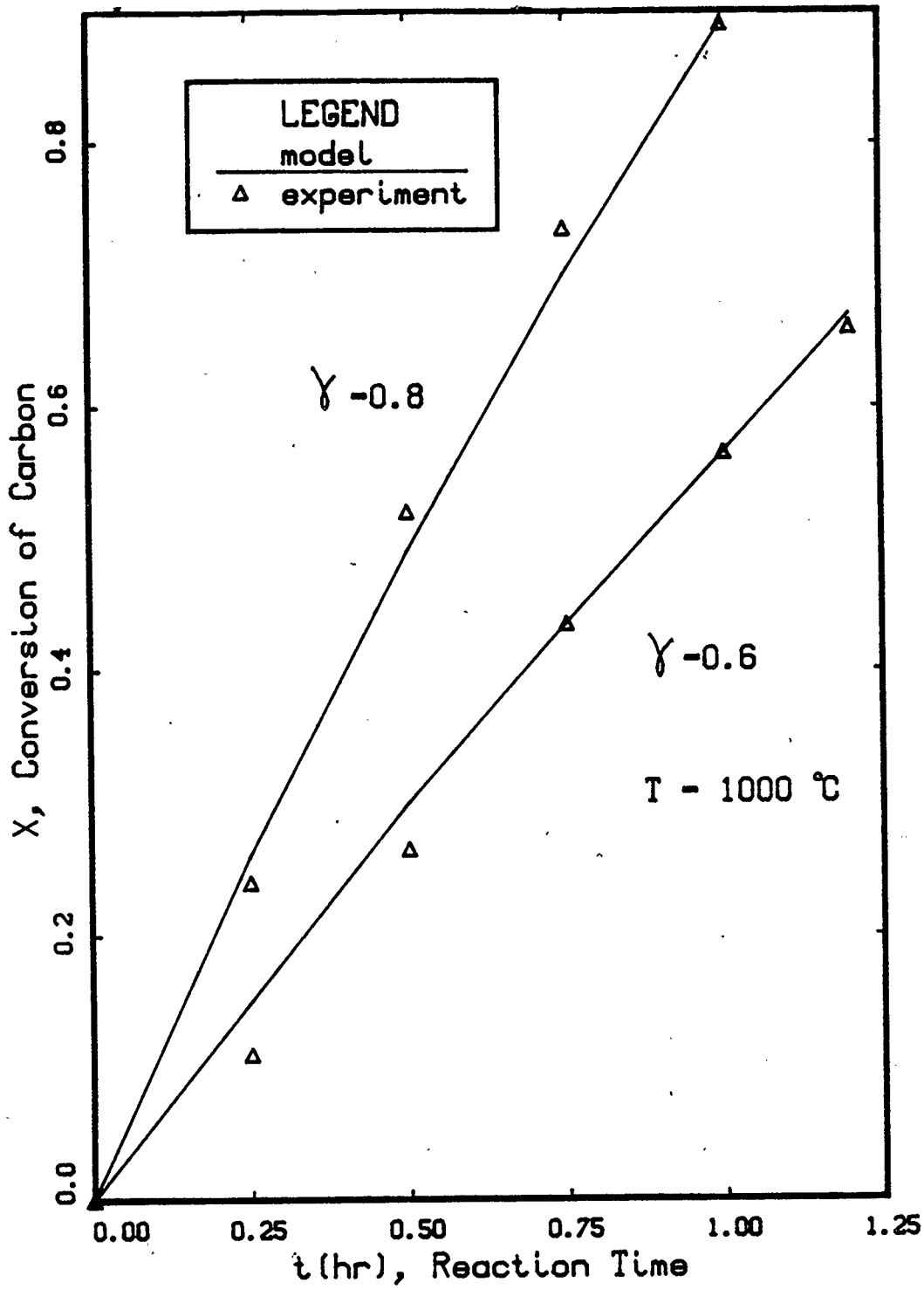

Figure 16 Conversion vs time, catalytic carbon gasification at 1000 °C

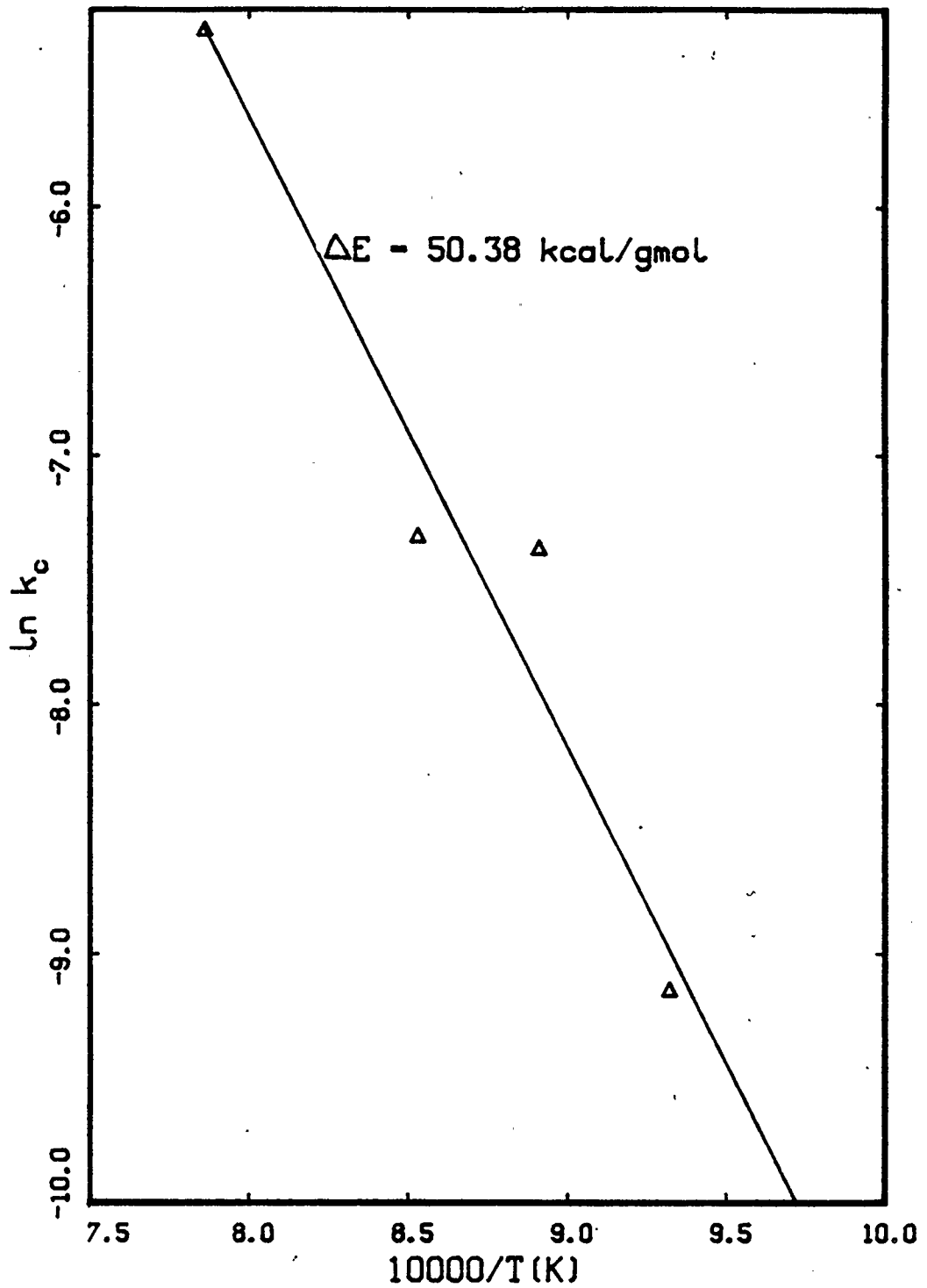

Figure 17 Arrhenius plot for rate constant k_c for catalytic carbon gasification

3. Comparison of Noncatalytic and Catalytic Carbon Gasification

Figure 18 shows a comparison of the conversion - time behaviour predicted by the single-reaction model for noncatalytic and catalytic carbon gasification (γ= 0.2, 0.8) at 1000°C. The trend exhibited in Figure 18 is indicative of the general trend at all temperatures investigated. The more catalyst present (at least up to γ = 0.8 - 1.0), the faster is the reaction rate. Indeed, this is expected. Figures 19 and 20 show the profiles of reactant gas concentrations and grain radii across the pellet. The figures show comparisons of the noncatalytic and catalytic systems at 1000°C and a conversion of 0.22. Since the conversion rates are different for the two systems, the times at which this conversion is reached are different (1.5 hours and 0.5 hours for the noncatalytic and catalytic system respectively).

The profiles through the pellet in both the catalytic and noncatalytic cases indicate that the reactions are controlled by both diffusion and kinetic resistances. If the reactions were diffusion controlled, the intrinsic rate of reaction would be faster than the rate of diffusion into the pellet. Any reactant gas diffusing into the pellet would be consumed at or near the pellet surface. Thus the concentration profile of the reactant gas would be very steep, with high concentrations (approaching bulk concentration) at the pellet (R/R_p = 1.0) which drop off to near zero a short distance into the pellet. The grain radius profile would also be very steep, with r_g approaching r_o (initial grain radius) a short distance into the

pellet. The grains at the center of the pellet would be essentially unreacted.

On the other hand, if the reactions had been kinetically controlled, the rate of diffusion into the pellet would have been greater than the intrinsic reaction rate. Thus the concentration profile of the reactant gas would be flat. The gas would diffuse far into the pellet before reaction consumed it. The reactant gas concentration would be nearly equal across the pellet. Reaction would occur simultaneously throughout the pellet and the grain radii would decrease at approximately the same rate. Thus the grain radius profile would also be flat.

Examination of Figures 19 and 20 shows that the concentration and grain radius profiles are between the two extremes discussed above. Therefore, the reactions are both kinetic and diffusion controlled. It can also be seen that the catalytic system exhibits much steeper profiles across the pellet than the noncatalytic system. This is the expected trend since the catalyst enhances the intrinsic reaction rate. Thus the overall reaction becomes more diffusion controlled as catalyst is added.

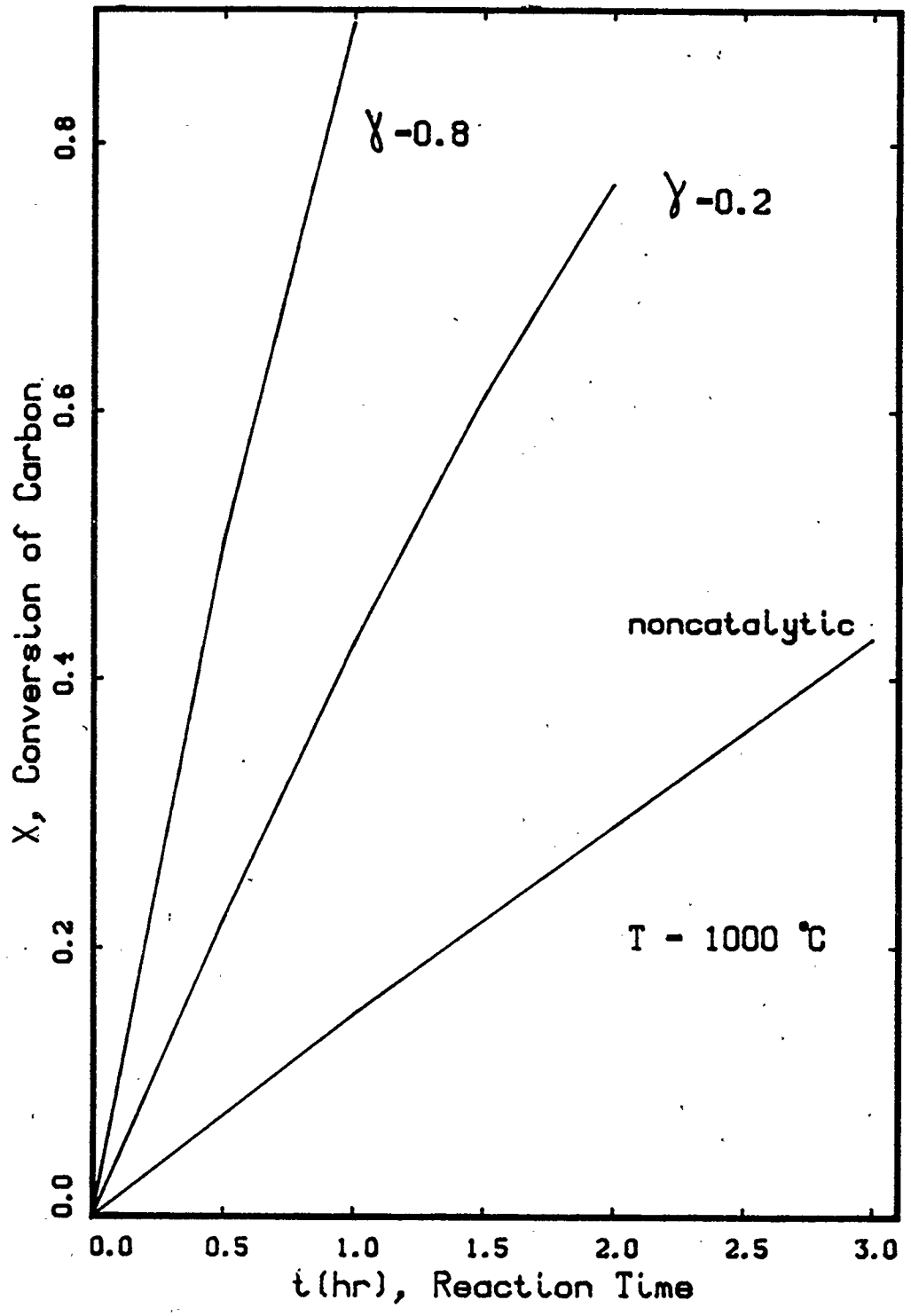

Figure 18 Conversion vs time, carbon gasification at 1000 °C

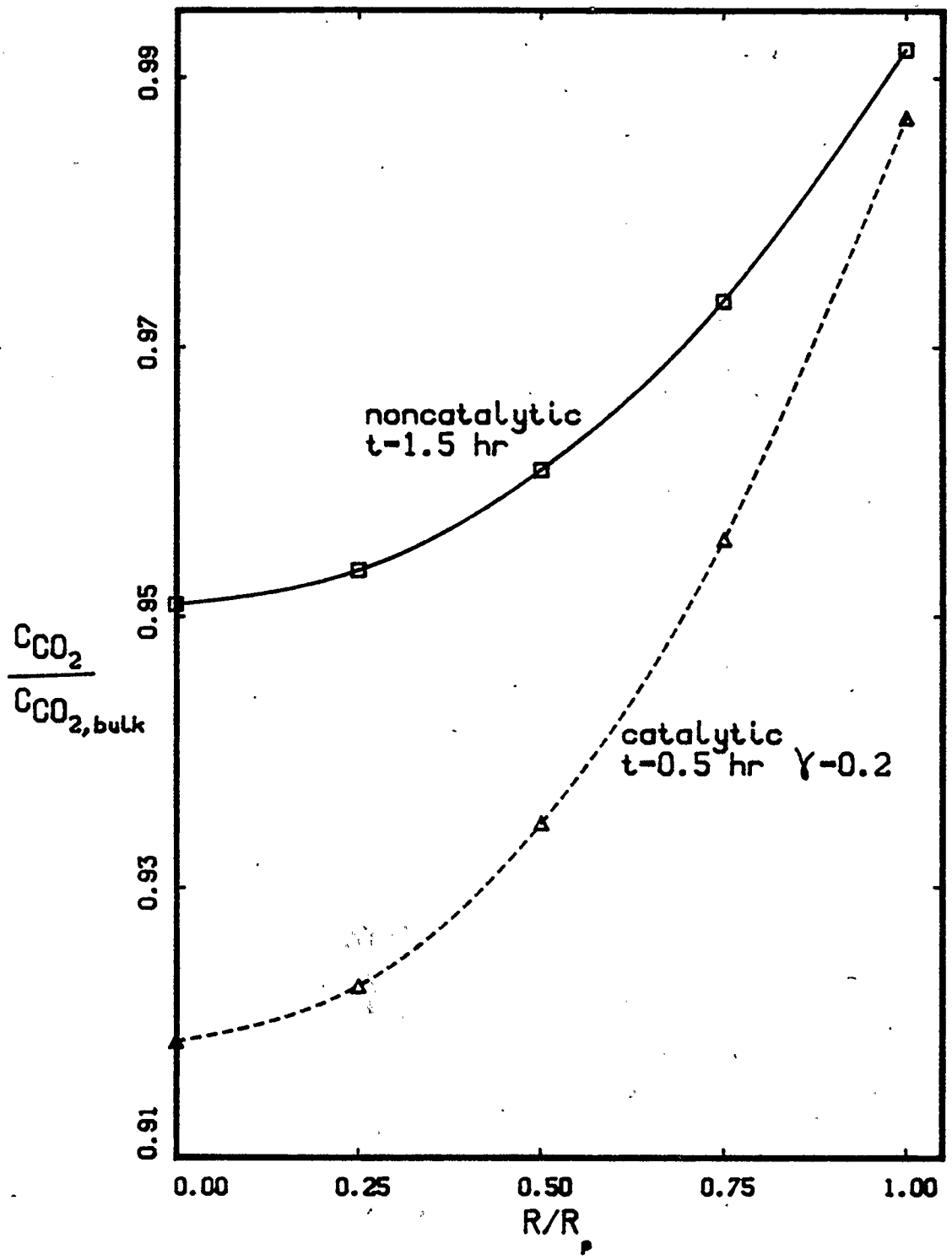

Figure 19 Concentration profile of reactant gas, T-1000 °C, conversion-0.22

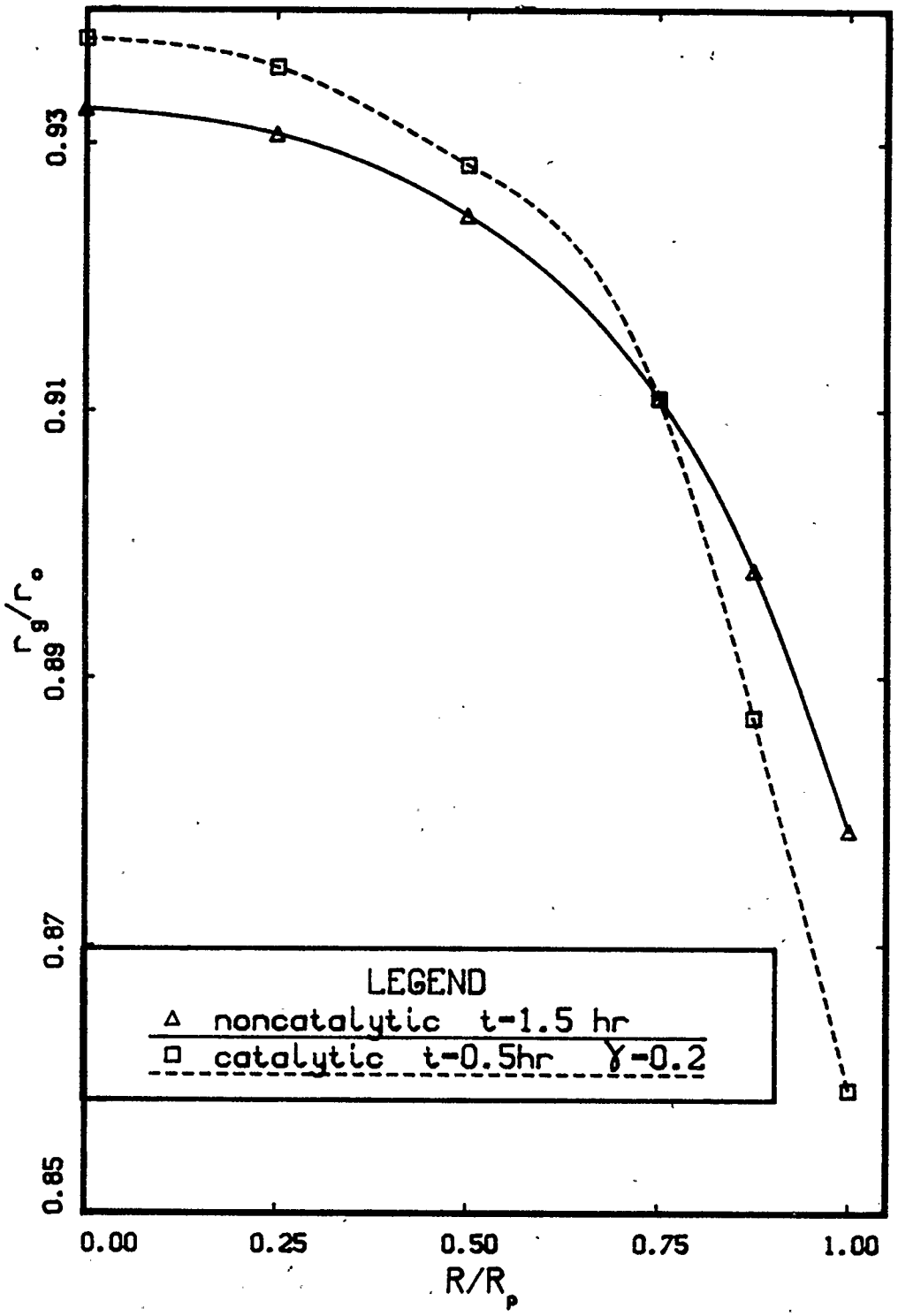

Figure 20 Grain radius profile, T=1000 °C conversion=0.22

C. NICKEL OXIDE REDUCTION

The final system with which the single-reaction model was tested is the reduction of nickel oxide with carbon monoxide. The governing reaction is described by the following equation:

$$NiO + CO \longrightarrow Ni + CO_2$$

The reaction is modelled with first order kinetics, ie:

$$\text{Rate} = k_{NiO} C_{CO}$$

The rate constant k_{NiO} was used to fit the model predictions to the experimental results at each temperature. As discussed for the previous systems, k_{NiO} at any given temperature was assumed constant and was not a function of conversion. All experimental parameters other than k_{NiO} were fixed. The values used for the experimental parameters are found in Appendix 3.

Experimental results [65] were available at five temperatures between 800°C and 1100°C; the model predictions of conversion - time behaviour were made at each temperature. Comparisons between

the model predictions and experimental results are shown in Figures 21 to 25. The match between model and experiment is excellent up to 80% conversion at all temperatures. Errors of only 5% are incurred up to 90% conversion at each temperature.

One difficulty that was encountered while modelling this system was the uncertainty of the initial grain radius of the nickel oxide grains. In the experimental work [65], it was determined only that the grain radius was less than 0.5 microns. Since the model requires a definite value of grain radius, an assumption had to be made about the value. The model was run using two different values of initial grain radius, values of 0.5 and 0.3 microns were used. It was found that essentially identical predictions of conversion - time behaviour could be produced for either grain radius, providing k_{NiO} was allowed to vary. Table 10 shows the values of k_{NiO} found for both grain radii at each of the five experimental temperatures.

Table 10 Rate Constant k_{NiO} for Two Sizes of Initial NiO Grain Radius

	$k_{NiO} \times 10^6$ (m/s)	
T(°C)	r_o = 0.5 m	r_o = 0.3 m
800	21.0	13.0
850	19.0	11.5
900	27.0	16.0
1000	18.0	11.0
1100	23.0	14.0

Values of k_{NiO} for a grain radius of 0.5 micron are 60% to 70% higher than k_{NiO} for r_o = 0.3 micron. At the higher grain radius, the value of k_{NiO} must be higher to give the same rate of conversion, since the surface area available for reaction in the pellet is smaller for larger grains.

The rate constant k_{NiO} is assumed to be an Arrhenius function of temperature. Figure 26 shows Arrhenius plots for grain radii of 0.5 and 0.3 micron respectively. Analysis of these plots results in activation energies of 461 cal/gmol for a grain radius of 0.5 micron and 208 cal/gmol for 0.3 micron. These values of activation energy are compared to literature values in Table 11. The small activiation energies explain why, at both values of r_o , the values of k_{NiO} do not change appreciably with temperature (i.e. k_{NiO} is essentially independent of temperature).

Table 11 Comparison of Activation Energy for Nickel Oxide Reduction

T range (°C)	Δ E (kcal/mole)	Reference
847 - 1099	4	70
682 - 796	≈0	71
800 - 1100	0.21 - 0.46	Present Study

The activation energies found for nickel-oxide reduction in this study fall within the range of values reported in the literature. However, they cannot be accepted with a high degree of confidence. Examination of Figure 26 shows that the data exhibits bad scattering.

This is thought to be caused be severe sintering in the nickel oxide reduction system. Sintering of the nickel product causes grain agglomeration and pore blockage which alters the diffusion processes in the pellet. Attempting to account for the effect of sintering is beyond the scope of this study. Thus meaningful Arrhenius plots cannot be produced by the model if sintering is occurring. In the experimental work [65], evidence of severe sintering is reported for the nickel oxide reduction system.

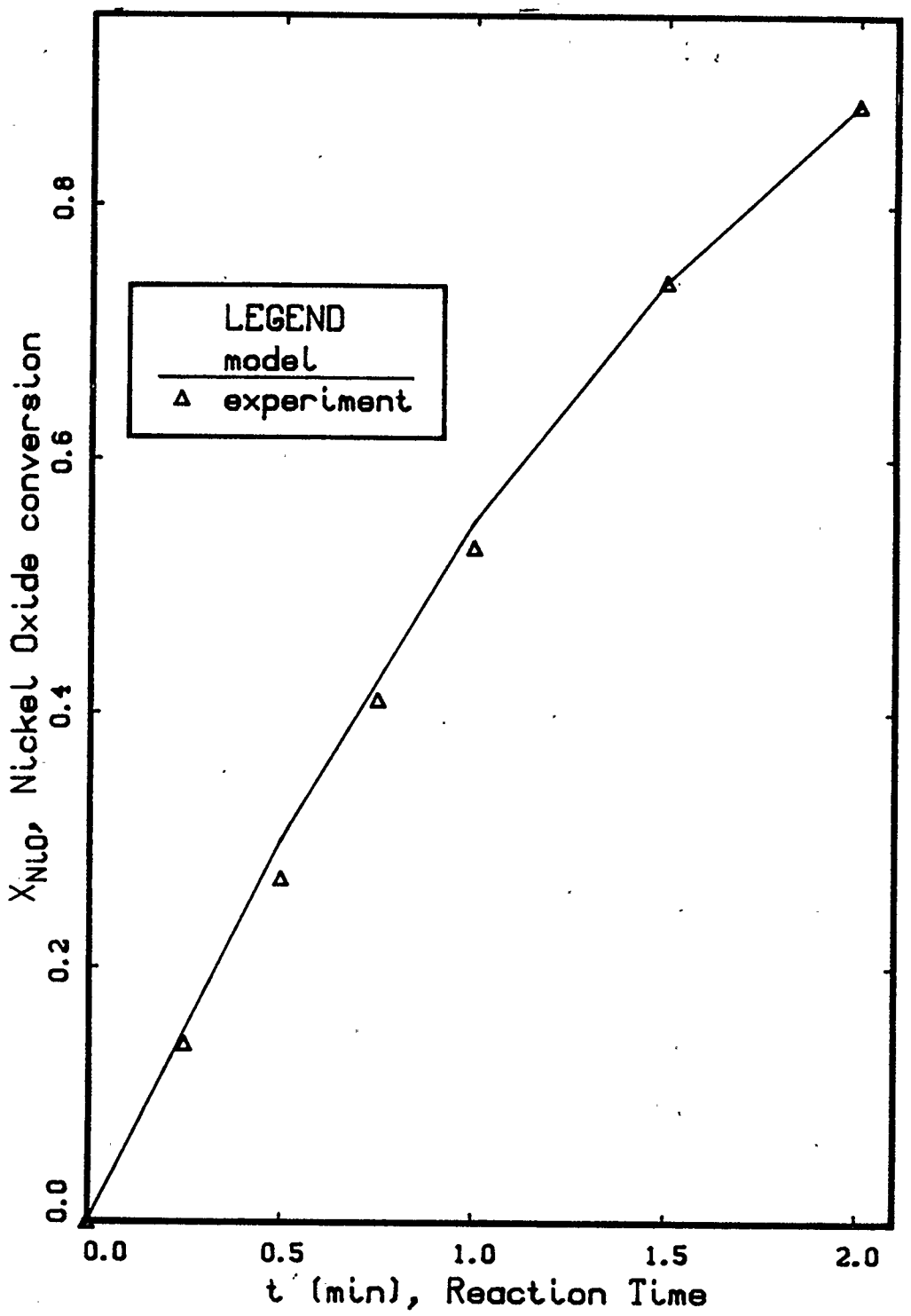

Figure 21 Conversion vs time, Nickel Oxide reduction, T-800 °C

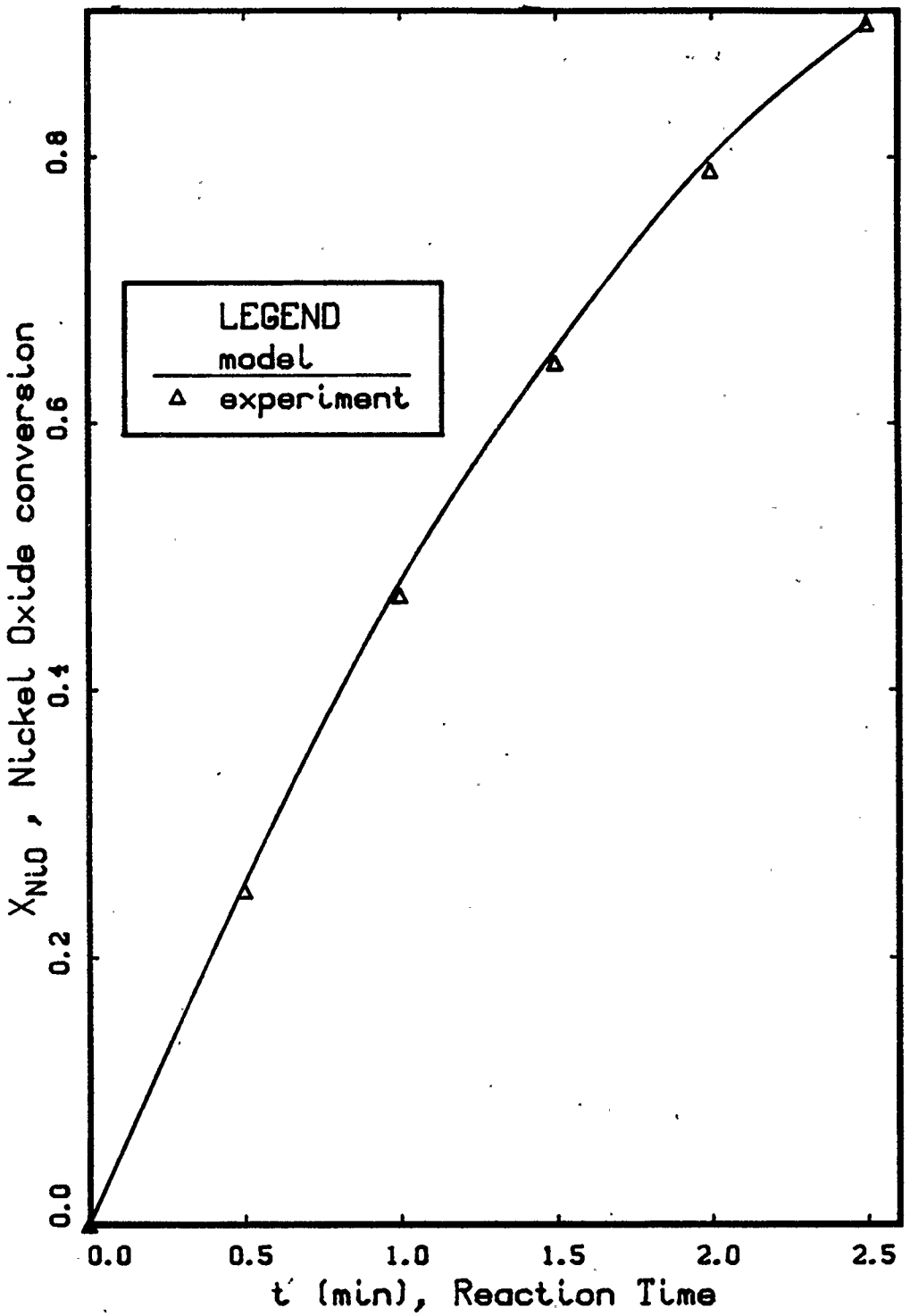

Figure 22 Conversion vs time, Nickel Oxide reduction, T-850 °C

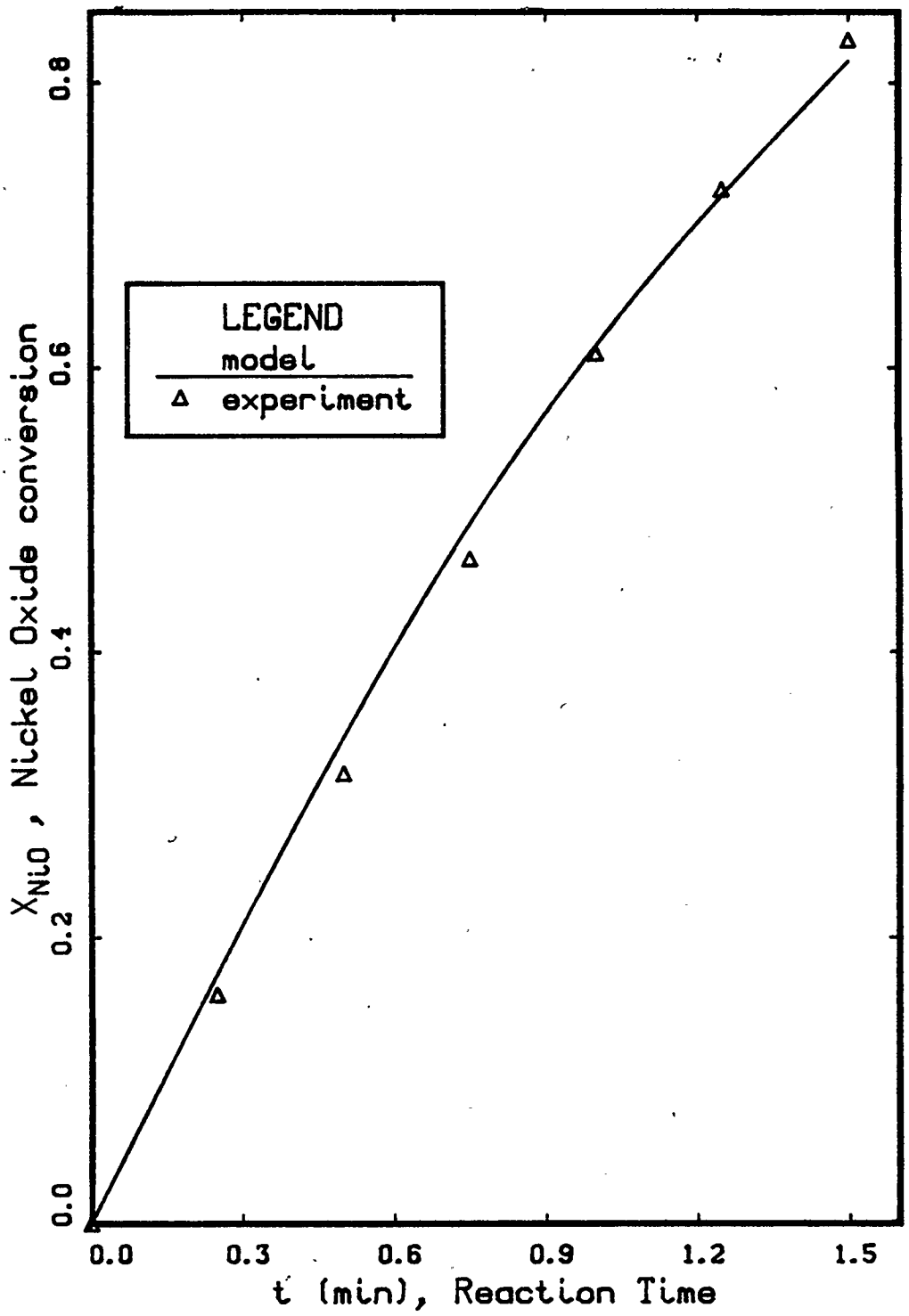

Figure 23. Conversion vs time, Nickel Oxide reduction, T=900 °C

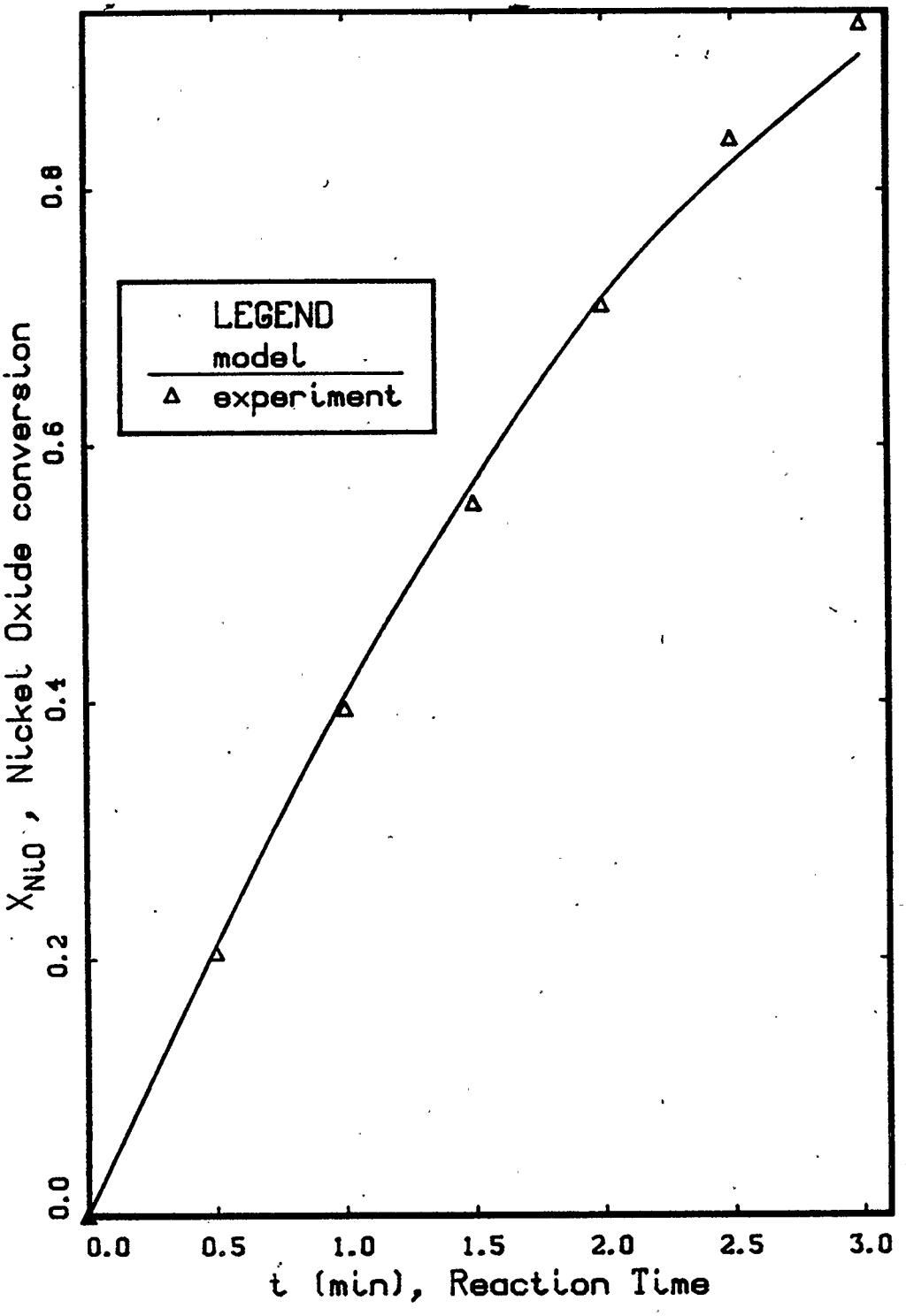

Figure 24 Conversion vs time, Nickel Oxide reduction, T-1000 °C

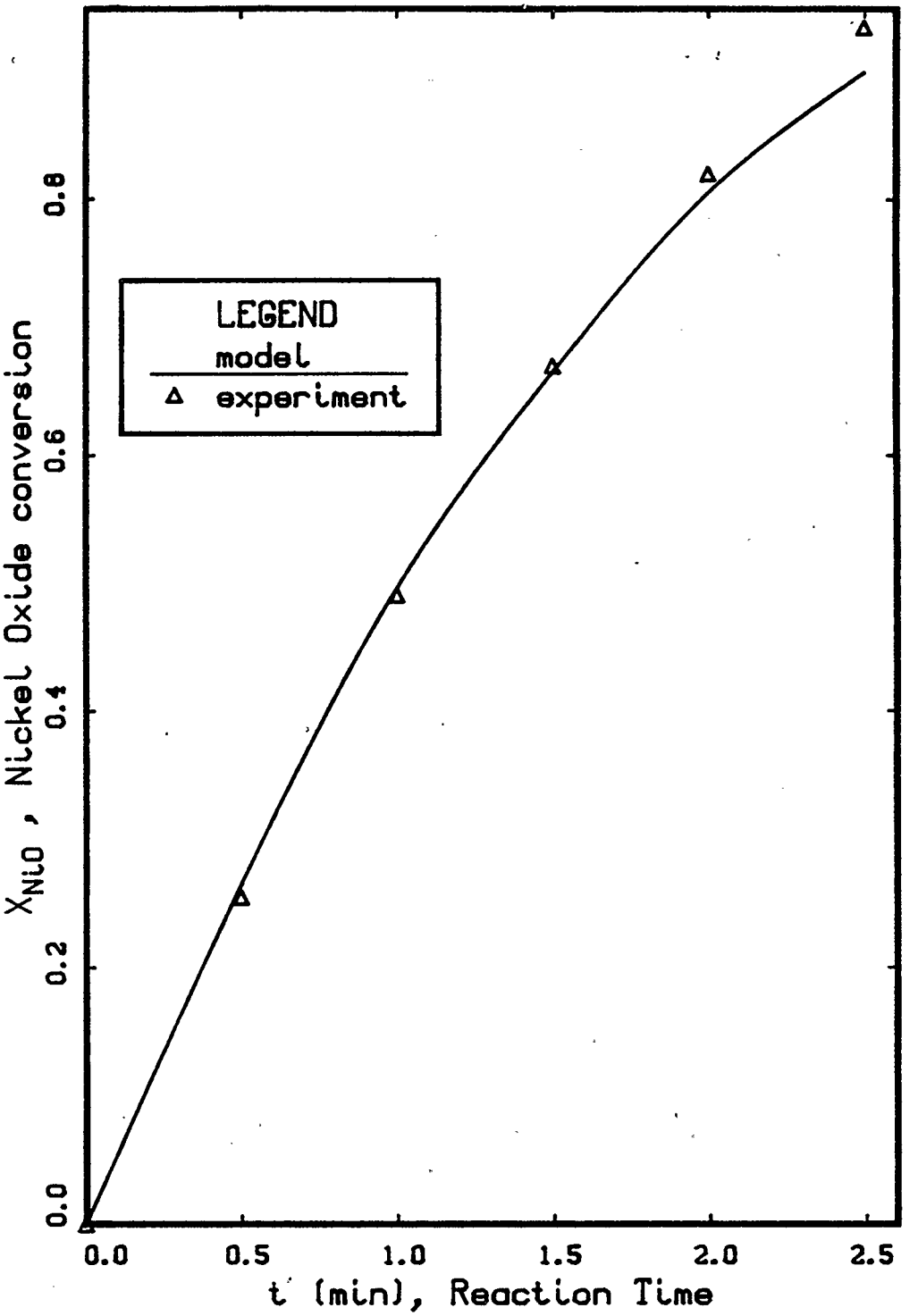

Figure 25 Conversion vs time, Nickel Oxide reduction, T=1100 °C

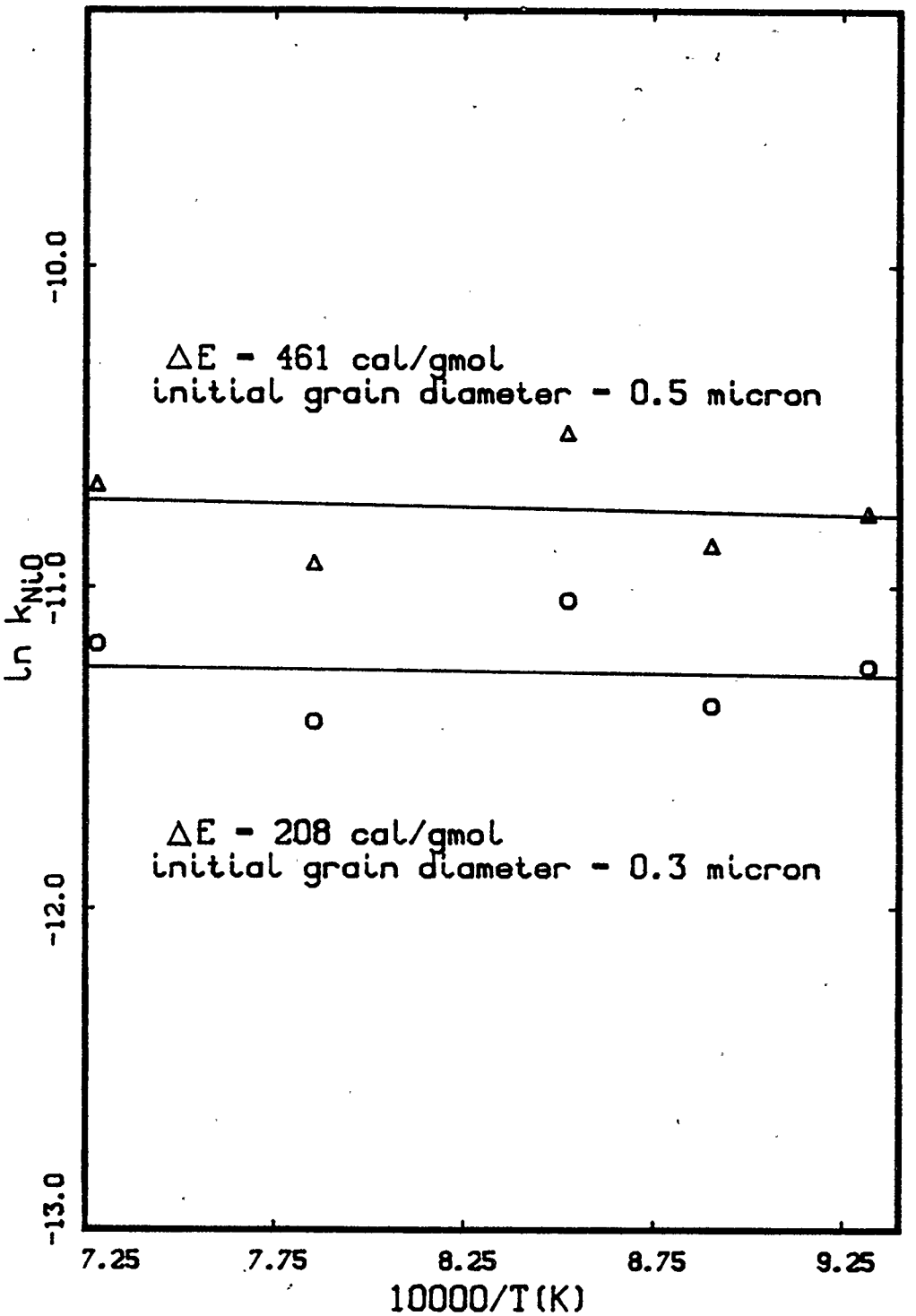

Figure 26 Arrhenius plot for k_{NiO}

D. MULTI-REACTION SYSTEM

The multi-reaction model was tested by comparing model predictions to experimental results for the carbon/nickel oxide/carbon dioxide system. The system is described by the following reactions:

$$C + CO_2 \longrightarrow 2CO$$

$$NiO + CO \longrightarrow Ni + CO_2$$

The carbon gasification reaction is catalyzed by the nickel which is produced by the nickel oxide reduction. The nickel oxide reacts with carbon monoxide which is produced by carbon gasification (ie. no CO is present in the bulk gas stream).

The rate of reaction for the catalytic carbon gasification is given by Langmuir - Hinshelwood kinetics:

$$\text{Rate} = \frac{(k_1 + k_c \rho_{Niapp}) P_{CO_2}}{1 + k_2 P_{CO} + k_3 P_{CO_2}}$$

Where ρ_{Niapp} is the apparent nickel density defined by the weight of nickel in the pellet per unit volume of pellet.

The nickel oxide reduction is governed by first order reaction kinetics:

$$\text{Rate} = k_{NiO} C_{CO}$$

The model was tested against experimental data for the system at reaction temperatures of 800 and 900°C. The reaction constants for the carbon gasification rate equation at the two reaction temperatures are given in Table 12 below.

Table 12 Rate constants for catalytic carbon gasification at 800°C and 900°C

Rate Constant	T = 800°C	T = 900°C
k_1(mol/atm m s)^2	0.65×10^{-8}	6.5×10^{-8}
k_c(mol m/atm kg s)	1.072×10^{-4}	6.616×10^{-4}
k_2(atm^{-1})	7256.0	643.0
k_3(atm^{-1})	3.951	3.031

Rate constants k_1 and k_c are those found in previous sections by fitting the single-reaction model predictions to experimental results. Constants k_2 and k_3 come from the work of Wu [85].

The rate constant for nickel oxide reduction, k_{NiO}, was obtained from the equation:

$$k_{NiO} = 2.072 \times 10^{-5} \exp(-461/R_g T) \text{ m/s}$$

An activation energy of 461 cal/mol was used as a result of setting the initial grain radius of nickel oxide grains to 0.5 micron.

Nickel was produced as the experiments proceeded; as a result, nickel (or catalyst) concentration changed with conversion. The apparent nickel density was calculated in the following manner:

$$\rho_{Niapp} = \rho_{Ni}\ \alpha_{Ni}$$

where ρ_{Ni} is the true nickel density (=8900 kg/m^3) and α_{Ni} is the apparent volume fraction of nickel at any time:

$$\alpha_{Ni} = \alpha_{NiO,initial} \frac{(r_{g,NiO} - r_{c,NiO})^3}{(r_{o,NiO})^3}$$

Experimental results [65] for the multi-reaction system indicated a very high rate of conversion at the beginning of the reaction (ie. within the first two minutes). This was explained to be the result of solid-solid reaction at the contact points of nickel oxide and carbon grains. The multi-reaction model developed in this study was not written to account for this initial, fast solid-solid reaction. To take into account the effect of the solid-solid reaction, the model predictions were started after two minutes of reaction time. In other words, the initial condition for the model was shifted to time = 2 minutes and total conversion

= the total conversion at 2 minutes as determined from the experimental results. Table 13 shows the values of total conversion after two minutes of reaction from the experimental results.

Table 13 Total Conversion after Two Minutes of Reaction Time

T (°C)	γ	X_T, total conversion
800	0.05	0.025
900	0.05	0.05
900	0.1	0.095

It can be seen that conversion in the first two minutes of reaction increases with temperature and with the ratio of nickel oxide to carbon grains.

Figure 27 shows comparisons of model predictions to experimental results for the three cases in Table 13. At 800°C and 0.05 moles nickel oxide per mole of carbon, the model prediction is good. At 900°C, however, the model predicts a much higher rate of conversion than the experimental results exhibit. It is postulated that sintering was occurring in the experimental system. The sintering of nickel as

it was produced would lower the effective concentration of the catalyst. Thus, the experimental conversion was not as fast as that predicted by the model (which does not include the effect of sintering).

For the two cases at 900°C, the model predictions were corrected empirically to fit the experimental results. The correction is based on decreasing the rate of increase of catalyst concentration. It is proposed that this is the same effect as sintering would have on the system. Additional study should be concentrated on incorporating the effect of sintering on the reaction system.

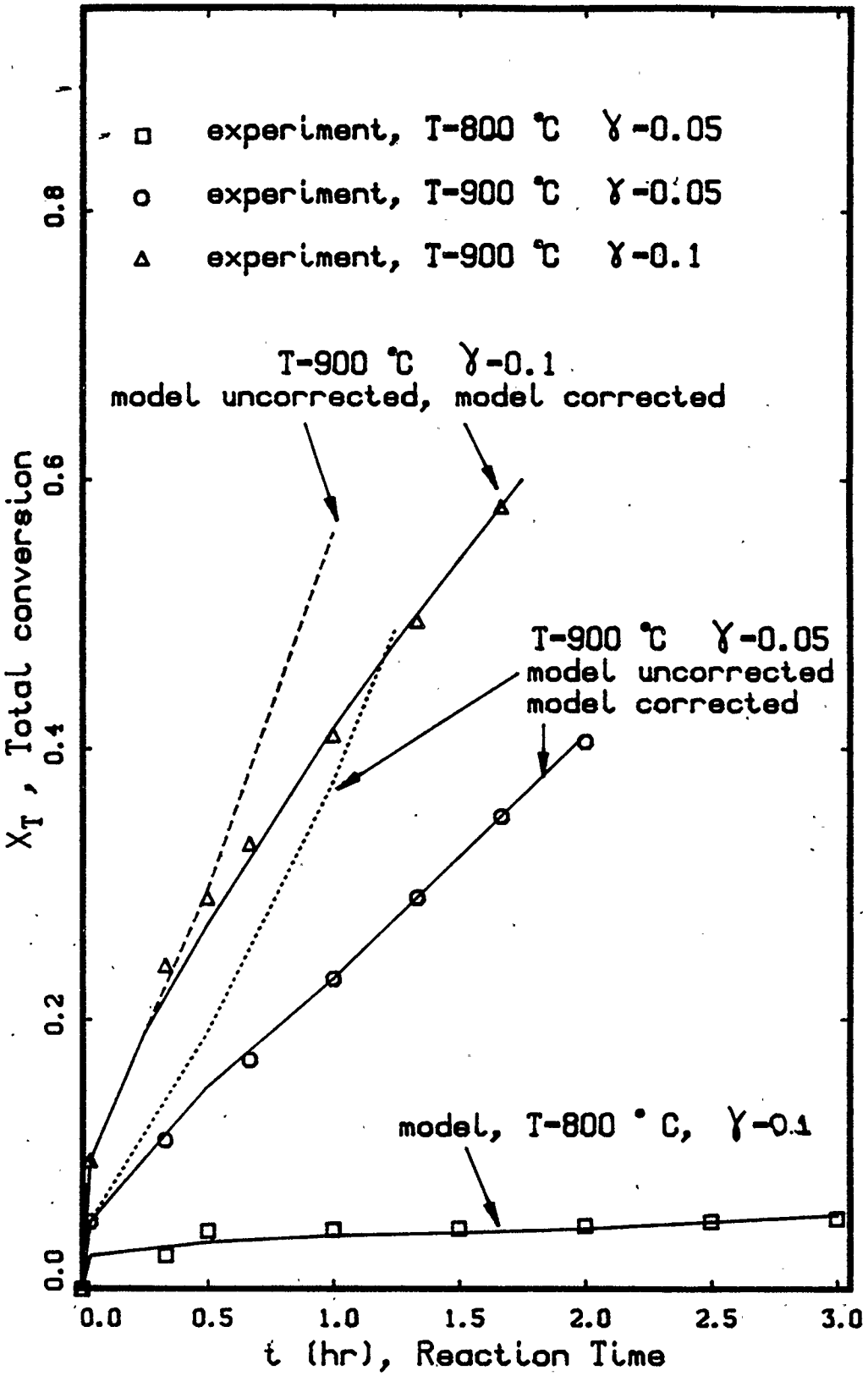

Figure 27 Total conversion vs time
multi-reaction system

VII CONCLUSIONS

1) The single-reaction model generates excellent predictions of conversion for single reactions which are well defined in terms of kinetics and pellet structure.

2) Simple non-catalytic carbon gasification with carbon dioxide can be predicted very well by the single reaction model.

3) Carbon gasification with carbon dioxide in the presence of metal catalysts can be predicted very well by the single -reaction model.

4) The catalytic effect of nickel was successfully incorporated into the model.

5) For reactions which experience an exposure time before becoming fully developed, the model can successfully predict conversion only in the fully developed region.

6) For reactions accompanied by severe structural changes which are not mathematically formulated (ie severe sintering), very good conversion predictions can be made by fitting kinetic parameters. However, meaningful Arrhenius activation energies can not be found.

7) The single-reaction model can be used in conversion predictions for processes such as coal gasification.

8) The single-reaction and multi-reaction models can be used to find optimum catalyst concentrations for reactions.

VIII RECOMMENDATIONS

1) Additional study should be concentrated on deriving a good mathematical formulation for sintering processes. This formulation should be incorporated into the models.

2) The catalytic effect of metals other than nickel on the carbon gasification reaction should be investigated.

3) The effect of solid-solid reactions should be investigated and incorporated into the multi-reaction model.

NOMENCLATURE

b stoichiometric coefficient for species B, moles B/mole A

C concentration of gas, mole/m^3

c stoichiometric coefficient for species C, moles C/mol A

D composite diffusivity accounting for Knudsen and molecular diffusion, m^2/s

D_{AC} molecular diffusivity for binary mixture A and C, m^2/s

D_e effective diffusivity, m^2/s

D_g effective diffusivity in the product layer surrounding grains, m^2/s

D_K Knudsen diffusivity, m^2/s

d stoichiometric coefficient for species D, moles D/mole A

d_p characteristic pore dimension, m

d_{pg} characteristic pore dimension in the product layer surrounding grains, m

F_p pellet shape factor

h external mass transfer coefficient, m/s

k_1, k_2, k_3 intrinsic rate constants for carbon gasification; mol/atm m^2 s, atm^{-1}, atm^{-1}

k_c catalytic rate constant for catalytic carbon gasification, $\frac{\text{mol m}}{\text{atm kg s}}$

k_{NiO} intrinsic rate constant for nickel-oxide reduction, m/s

M molecular weight, kg/kmol

N molar flux, mol/m^2s

n number of moles

n_g number of grains

P pressure, atm

P_c critical pressure, atm

P_v Volume of pore space per grain, m^3

R distance coordinate in the pellet, m

Re Reynolds number, = $R_p \mu \rho / \mu$

R_g universal gas constant

R_p pellet characteristic dimension, m

r_c radius of reaction front in grain, m

r_g grain radius at any time, m

r_o initial grain radius, m

Sc Schmidt number, = $\mu / \rho D_{AC}$

S_E surface area of the volume element, m^2

Sh Sherwood number, = $h R_p / D_{AC}$

S_v surface area in the pellet available for reaction per unit volume of pellet, m^{-1}

T reaction temperature, K

T_c critical temperature, K

T_r reduced temperature, ($= T/T_c$)

t time, s

u velocity, m/s

V_E volume of element, m^3

X overall conversion

x local conversion

x_A, x_C mole fraction of species A and C respectively

GREEK LETTERS

α volume fraction of solid in pellet

γ molar ratio of Ni(or NiO) to C present in pellet,

$$\frac{\text{moles Ni(or NiO)}}{\text{mole C}}$$

ε pellet porosity

ε_D, ε_E porosity in the product layer surrounding grains

μ viscosity, kg/ms

ρ true solid density, kg/m^3

ρ_{Niapp} apparent nickel density, kg/m^3

τ tortuosity

SUBSCRIPTS

A gaseous species A

B solid species B

b bulk fluid stream

C fluid species C

D solid species D

E solid species E

i reaction interface in grain

o initial value

T total

REFERENCES

1) Ramachandran, P.A., L.K. Doraiswamy, "Modeling of Noncatalytic Gas - Solid Reactions," AIChE J., 28, No. 6, p. 881 (1982)

2) Yagi, S., D. Kunii, "Fluidized - solids reactors with continuous solids feed - I," Chem. Eng. Sci., 16, p. 365 (1961)

3) Levenspiel, O., Chemical Reaction Engineering, Wiley, N.Y., (1962)

4) Szekely, J., J.W. Evans, H.Y. Sohn, Gas - Solid Reactions, Academic Press, N.Y., (1976)

5) Erk, H.F., M.P. Dudukovic, "Self - Inhibited Rate in Gas - Solid Noncatalytic Reactions: The "Rotten Apple" Phenomenon and Multiple Reaction Pathways," Ind. Eng. Chem. Fundam., 22, p. 55, (1983)

6) Rehmat, A., S.C. Saxena, R. Land, A.A. Jonke, "Noncatalytic Gas - Solid Reaction with Changing Particle Size: Unsteady State Heat Transfer," Can. J. Chem. Eng., 56, p. 316 (1978)

7) Dudukovic, M.P., "Reactions of Particles with Nonuniform Distribution of Solid Reactant. The Shrinking Core Model," Ind. Eng. Chem. Process Des. Dev., 23, p. 330, (1984)

8) Park, J.Y., O. Levenspiel, "The Crackling Core Model for the Reaction of Solid Particles," Chem. Eng. Sci., 30, p. 1207, (1975)

9) Ramachandran, P.A., M.P. Dudukovic, "Reactions of Solid Particles with Nonuniform Distribution of Solid Reactant: The Volume Reaction Model," Chem. Eng. Sci., 39, p. 669, (1984)

10) Kimura, S., J. Nakagawa, S. Tone, T. Otake, "The Volume Reaction Model Based on a Second Order Rate Equation and its Application to a Gas - Solid Reaction" J. Chem. Eng. Japan, 14, p. 190, (1981)

11) Ishida, M., C.Y. Wen, "Comparison of Kinetic and Diffusional Models for Gas - Solid Reactions," AIChE J., 14, p. 311 (1968)

12) Ishida, M., C.Y. Wen, "Comparison of Kinetic and Diffusional Models for Gas - Solid Reactions," Chem. Eng. Sci., 26, p. 1031, (1971)

13) Ishida, M., C.Y. Wen, T. Shirai, "Comparison of Zone - Reaction Model and Unreacted - Core Shrinking Model in Solid - Gas Reaction - II: Non-isothermal Analysis," Chem. Eng. Sci., 26, p. 1043, (1971)

14) Lone, S., C.Y. Wen, "Application of the Zone Model to Multiple Noncatalytic Fluid - Solid Reactions," Chem. Eng. Sci., 36, p. 273, (1981)

15) Mantri, V.B., A.N. Gokarn, L.K. Doraiswamy, "Analysis of Gas - Solid Reactions: Formulation of a General Model," Chem. Eng. Sci., 31, p. 779, (1976)

16) Bowen, J.H., C.K. Cheng, "A Diffuse Interface Model for Fluid - Solid Reaction," Chem. Eng. Sci., 24, p. 1829, (1969)

17) Prasannan, P.C., L.K. Doraiswamy, "Gas - Solid Reactions: Experimental Evaluation of the Zone Model," Chem. Eng. Sci., 37, p. 925, (1982)

18) Ramachandran, P.A., L.K. Doraiswamy, "Analysis of Gas - Solid Reactions with Zero - Order Dependency on Gas and Solid: Concept of Jumping Reaction Zones," AIChE J., 30, p. 637, (1984)

19) Petersen, E.E., "Reaction of Porous Solids," AIChE J., 3, p. 443, (1957)

20) Ramachandran, P.A., J.M. Smith, "A Single - Pore Model for Gas - Solid Noncatalytic Reactions," AIChE J., 23, p. 353, (1977)

21) Ulrichson, D.L., D.J. Mahoney, "Pore Closure Models for Gas - Solid Reactions: The Effect of Bulk Flow and Reversibility," Chem. Eng. Sci., 35, p. 567, (1980)

22) Hashimoto, K., P.L. Silveston, Gasification: Part 1. Isothermal, Kinetic Control Model for a Solid with a Pore Size Distribution," AIChE J., 19, p. 259, (1973)

23) Gavalas, G.R., "A Random Capillary Model with Application to Char Gasification at Chemically Controlled Rates," AICHE J., 26, p. 577, (1980)

24) Bhatia, S.K., D.D. Perlmutter, "A Random Pore Model for Fluid - Solid Reactions: I. Isothermal, Kinetic Control," AIChE J., 26, p. 379 (1980)

25) Bhatia, S.K., D.D. Perlmutter, "A Random Pore Model for Fluid - Solid Reactions: II. Diffusion and Transport Effects," AIChE J., 27, p. 247, (1981)

26) Bhatia, S.K., D.D. Perlmutter, "The Effect of Pore Structure on Fluid - Solid Reactions: Application to the SO_2 - Lime Reaction," AIChE J., 27, p. 226, (1981)

27) Bhatia, S.K., D.D. Perlmutter, "Effect of the Product Layer on the Kinetics of the CO_2 - Lime Reaction," AIChE J., 29, P. 79, (1983)

28) Su, J.L., D.D. Perlmutter, "Effect of Pore Structure on Char Oxidation Kinetics," AIChE J., 31, p. 973, (1985)

29) Su, J.L., D.D. Perlmutter, "Evolution of Pore Volume Distribution During Gasification," AIChE J., 30, p. 967, (1984)

30) Bhatia, S.K., Analysis of Distributed Pore Closure in Gas - Solid Reactions," AIChE J., 31, p. 642, (1985)

31) Szekely, J., J.W. Evans, "A Structural Model for Gas - Solid Reactions with a Moving Boundary," Chem. Eng. Sci., 25, p. 1091, (1970)

32) Szekely, J., J.W. Evans, "Studies in Gas - Solid Reactions: Part 1. A Structural Model for the Reaction of Porous Oxides with a Reducing Gas," Met. Trans., 2, p.1691, (1971)

33) Szekely, J., H.Y. Sohn, "Effect of Structure on the Reaction Between a Porous Solid and a Gas," Inst. Mining & Metallurgy, Trans./Sec.C., 82, p. C92, (1973)

34) Szekely, J., J.W. Evans, "A Structural Model for Gas - Solid Reactions with a Moving Boundary - II: The Effect of Grain Size, Porosity and Temperature on the Reaction of Porous Pellets," Chem. Eng. Sci., 26, p. 1901, (1971)

35) Sohn, H.Y., J. Szekely, "A Structural Model for Gas - Solid Reactions with a Moving boundary - III: A General Dimensionless Representation of the Irreversible Reaction Between a Porous Solid and a Reactant Gas," Chem. Eng. Sci.,27, p. 763, (1972)

36) Szekely, J., M.A. Hastaoglu, "Reduction of Nickel oxide - Hematite Mixtures with Hydrogen," Inst. Mining & Metallurgy, Trans./Sec.C, 85, p. C78, (1976)

37) Sohn, H.Y., J. Szekely, "The Effect of Reaction Order in Non-catalytic Gas - Solid Reactions," Can. J. of Chem. Eng., 50, p. 674, (1972)

38) Sohn, H.Y., J. Szekely, "A Structural Model for Gas - Solid Reactions with a Moving Boundary - IV: Langmuir - Hinshelwood Kinetics," Chem. Eng. Sci., 28, p. 1169, (1973)

39) Ramachandran, P.A., J.M. Smith, "Effect of Sintering and Porosity Changes on Rates of Gas - Solid Reactions," Chem. Eng. J., 14, p. 137, (1977)

40) Sohn, H.Y., J. Szekely, "The Effect of Intragrain Diffusion on the Reaction Between a Porous Solid and a Gas," Chem. Eng. Sci., 29, p. 630, (1974)

41) Sampath, B.S., P.A. Ramachandran, R. Hughes, "Modelling of Non-Catalytic Gas - Solid Reactions - I. Transient Analysis of the Particle - Pellet Model," Chem. Eng. Sci., 30, p. 125, (1975)

42) Szekely, J., M. Propster, A Structural Model for Gas - Solid Reactions with a Moving Boundary - VI: The Effect of Grain Size Distribution on the Conversion of Porous Solids," Chem. Eng. Sci., 30, p. 1049, (1975)

43) Sohn, H.Y., H. Sohn, "The Effects of Bulk Flow Due to Volume Change in the Gas Phase on Gas - Solid Reactions: Initially Nonporous Solids," Ind. Eng. Chem. Process Des. Dev., 19, p. 237, (1980)

44) Sohn, H.Y., O.A. Bascur, "Effect of Bulk Flow Due to Volume Change in the Gas Phase on Gas - Solid Reactions: Initially Porous Solids," Ind. Eng. Chem. Process Des. Dev., 21, 4, p. 658, (1982)

45) Sohn, H.Y., R.L. Braun, "Effect of Internally Generated Bulk Flow on the Rates of Gas - Solid Reactions. 1. Development of an

Approximate Solution," Ind. Eng. Chem. Process Des. Dev., 23, p. 685, (1984)

46) Sohn, H.Y., R.L. Braun, "Effect of Internally Generated Bulk Flow on the Rates of Gas - Solid Reactions. 2. Multiple Gas - Solid Reactions during the Gasification of Char in an Oil Shale Block," Ind. Eng. Chem. Process Des. Dev., 23, p. 691, (1984)

47) Calvelo, A., R.E. Cunningham, "Kinetics of Gas - Solid Reactions: Influence of Surface Area and Effective Diffusivity Profiles," J. of Catalysis, 17, p. 1, (1970)

48) Kim, K.K., J.M. Smith, "Diffusion in Nickel Oxide Pellets - Effects of Sintering and Reduction," AIChE J., 20, p. 670, (1974)

49) Georgakis, C., C.W. Chang, J. Szekely, "A Changing Grain Size Model for Gas - Solid Reactions," Chem. Eng. Sci., 34, p. 1072, (1979)

50) Garza-Garza, O., M.P. Dudukovic, "Some Observations on Gas - Solid Noncatalytic Reactions with Structural Changes," Chem. Eng. Sci., 36, p. 1257, (1981)

51) Garza-Garza, O., M.P. Dudukovic, "A Variable Size Grain Model for Gas - Solid Reactions with Structural Changes," Chem. Eng. J., 24, p. 35, (1982)

52) Ranade, P.V., D.V. Harrison, "The Grain Model Applied to Porous Solids with Varying Structural Properties," Chem. Eng. Sci., 34, p. 427, (1979)

53) Lindner, B., D. Simonsson, "Comparison of Structural Models for Gas - Solid Reactions in Porous Solids Undergoing Structural Changes," Chem. Eng. Sci., 36, p. 1519, (1981)

54) Sohn, H.Y., R.L. Braun, "Simultaneous Fluid - Solid Reactions in Porous Solids: Reactions Between One Solid and Two Fluid Reactants," Chem. Eng. Sci., 35, p. 1625, (1980)

55) Sohn, H.Y., R.L. Braun, "Simultaneous Fluid - Solid Reactions in Porous Solids - II. Reaction Between One Fluid and Two Solid Reactants," Chem. Eng. Sci., 39, p. 21, (1984)

56) Prassannan, P.C., P.A. Ramachandran, L.K. Doraiswamy, "A Model for Gas - Solid Reactions with Structural Changes in the Presence of Inert Solids," Chem. Eng. Sci., 40, p. 1251, (1985)

57) Reif, A.E., "The Mechanism of the Carbon Dioxide - Carbon Reaction," J. Phys. Chem., 56, p. 785 (1952)

58) Gadsby, J. , F.J. Long, P. Sleightholm, K.W. Sykes, "The Mechanism of the Carbon Dioxide - Carbon Reaction," Proc. Roy. Soc. (London), A193, p. 357 (1948)

59) Ergun, S., "Kinetics of the Reaction of Carbon Dioxide with Carbon," J. Phys. Chem., 60, p.480, (1956)

60) Grabke, H.J., "Oxygen Transfer and Carbon Gasification in the Reaction of Different Carbons with CO_2," Carbon, 10, p. 587, (1972)

61) Rao, Y.K., B.P. Jalan, "A Study of the Rates of Carbon - Carbon Dioxide Reaction in the Temperature Range 839° to 1,050°C," Met. Trans., 3, p. 2465 (1972)

62) Holstein, W.L., M. Boudart, "Uncatalyzed and Platinum - Catalyzed Gasification of Carbon by Water and Carbon Dioxide," J. of Catalysis, 75, p. 337, (1982)

63) Freund, H., "Kinetics of Carbon Gasification by CO_2," Fuel, 64, p. 657, (1985)

64) Adanez, J., J.L. Miranda, J.M. Gavilan, "Kinetics of a Lignite - Char Gasification by CO_2," Fuel, 64, p. 801, (1985)

65) Hastaoglu, M.A., "Study of NiO/C Composites in CO, CO_2 and N_2 Atmospheres," PhD. Thesis, State University of New York at Buffalo, (1976)

66) Walker, P.L., M. Shelef, R.A. Anderson, "Catalysis of Carbon Gasification," Chem. and Phys. of Carbon, 4, p. 287 (1968)

67) Long, F.J., K.W. Sykes, "The Catalysis of the Oxidation of Carbon," J. Chem. Phys., 47, p. 361, (1950)

68) Pettit, F., R. Yinger, J.B. Wagner, Acta Metallurgica, 8, p. 617 (1960)

69) Rakszawski, J.F., F. Rusinko, P.L. Walker, "Catalysis of the Carbon - Carbon Dioxide Reaction by Iron," Proc. 5th Carbon Conf., 2, p. 243, (1963)

70) Szekely, J., C.I. Lin, "The Reduction of Nickel Oxide Discs with Carbon Monoxide," Met. Trans., 7B, p. 493, (1976)

71) Krasuk J.H., J.M. Smith, "Kinetics of Reduction of Nickel Oxide with CO," AIChE J., 18, No. 3, p. 507, (1972)

72) Oates, W.A., D.D. Todd, "Kinetics of the Reduction of Oxides," J. Australian Inst. of Metals, 7, No. 2, p. 109, (1962)

73) Bielanski, A. , R. Dziembaj, H. Urbanska, "Reactions of Carbon Monoxide at the Surface of Nickel Oxide," Bull. Acad. Pol. Sci. Ser. Chim., 19, p. 447, (1971)

74) Mine, H., M. Tokuda, M. Ohtani, Nippon Kinzoku Gakkaishi, 34, No. 8, p. 814, (1970)

75) Rao, Y.K., "Investigation of the Mechanism of Carbon Reduction of Nickel and Copper Oxides," Met. Trans., 2, p. 1439, (1971)

76) Pavlyuchenko, M.M., I.F. Kononyuk, A.E. Pereverzev, "The Kinetics of Reduction of Hematite by Carbon," Izv. Akad. Nauk SSSR, Metal, 5, p. 147, (1967)

77) El-Guindy, M.I., W.G. Davenport, "Kinetics and Mechanism of Ilmenite Reduction with Graphite," Met. Trans., 1, p. 1729, (1970)

78) Yun, T.S., "Direct Reduction of Ferric Oxide by Solid Carbon in Vacuum," Trans. of the ASM., 54, p. 129, (1961)

79) Wakao, N., J.M. Smith, "Diffusion in Catalyst Pellets," Chem. Eng. Sci., 17, p. 825, (1962)

80) Rothfeld, L.B., AIChE J., 9, p. 19, (1963)

81) Bird R.B., W.E. Stewart, E.N. Lightfoot, Transport Phenomena, Wiley, N.Y., (1960)

82) Treybal, R.E., Mass Transfer Operations, 3rd Ed., McGraw-Hill, N.Y., (1980)

83) Rowe, P.N., K.T. Claxton, Trans. Inst. Chem. Eng., 43, p. T231, (1965)

84) Reid, R.C., T.K. Sherwood, The Properties of Gases and Liquids, McGraw - Hill, N.Y., (1977)

85) Wu, P.C., D. Sc. Thesis, M.I.T., Cambridge, (1949)

86) Lin, C.I., Ph.D. Thesis, State University of New York at Buffalo, (1975)

87) Lewis, W.K., R.G. Gilliland, G.J. McBride, "Modelling of Coupled Gas - Solid Reactions," Ind. Eng. Chem., 41, p. 1213, (1949)

88) Satterfield, C.N., Heterogeneous Catalysis in Practice, McGraw-Hill, N.Y., (1980)

89) Boikess, R.S., E. Edelson, Chemical Principles, Harper & Row, N.Y., (1978)

APPENDIX 1

Experimental Data - Noncatalytic Carbon Gasification

$C_{CO\ bulk} = 0.0$

Pressure = 1.0 atm

$\varepsilon_o = 0.566$

Bulk gas stream velocity = 5 l/min at 70°F and 1 atm

r_o(carbon) = 3.75 x 10^{-8} m

T(°C)	$R_n x10^2$ m	$^*C_{CO_2\ bulk}$ x10^6 mol/m^3
800	0.1448	11.36
850	0.1105	10.85
900	0.1041	10.39
1000	0.1778	9.57
1100	0.1283	8.88

$^*C_{CO_2\ bulk} = P/R_gT$

APPENDIX 2

Experimental Data - Catalytic Carbon Gasification

$C_{CO\ bulk} = 0.0$

Pressure = 1.0 atm

$\varepsilon_o = 0.55$

Bulk gas stream velocity = 5 l/min at 70°F and 1 atm

r_o(carbon) = 3.75 x 10 $^{-8}$ m

r_o(nickel) = 0.45 x 10 $^{-6}$ m

T(°C)	γ $\frac{\text{(mole Ni)}}{\text{(mol C)}}$	ρ_{Niapp} (g/cm^3)	$R_p x 10^2$ m
800	0.05	0.00326	0.1016
800	0.1	0.00625	0.0889
800	0.2	0.01094	0.0978
800	0.4	0.01786	0.0889
800	0.6	0.02197	0.1054
850	0.05	0.00327	0.0902
850	0.1	0.00616	0.1118
850	0.2	0.01120	0.0610
900	0.1	0.00623	0.1080
900	0.2	0.01104	0.1143
900	0.4	0.01801	0.0864
900	0.6	0.02244	0.0749
900	0.8	0.02453	0.1118
1000	0.05	0.00321	0.1461
1000	0.2	0.01095	0.1334
1000	0.4	0.01825	0.1029
1000	0.6	0.02210	0.1111
1000	0.8	0.02473	0.1308
1000	1.0	0.02810	0.1397

APPENDIX 3

Experimental Data - Nickel Oxide Reduction

$C_{CO_2\ bulk} = 0.0$
Pressure = 1.0 atm
$\varepsilon_0 = 0.55$
Bulk gas stream velocity = 16 l/min at 70°F and 1 atm

T(°C)	R_p x10^4 m	$C^*_{CO_2\ bulk}$ x10^6 mol/m^3
800	5.91	11.36
850	7.37	10.85
900	5.60	10.39
1000	8.76	9.57
1100	6.10	8.88

APPENDIX 4

Experimental Data - Multi-reaction System

$C_{CO\ bulk} = 0.0$

Pressure = 1.0 atm

Bulk gas stream velocity = 6 l/min at 70°F and 1 atm

T(°C)	γ	α_{Bo}	α_{Do}	$R_p \times 10^2 m$
800	0.05	0.416	0.034	0.0927
900	0.05	0.416	0.034	0.0673
900	0.1	0.387	0.063	0.0673